SAND76-0130
Unlimited Release
UC-60

Wind Tunnel Performance Data for the Darrieus Wind Turbine with NACA 0012 Blades

Bennie F. Blackwell, Robert E. Sheldahl, Louis V. Feltz

Sandia Laboratories
energy report

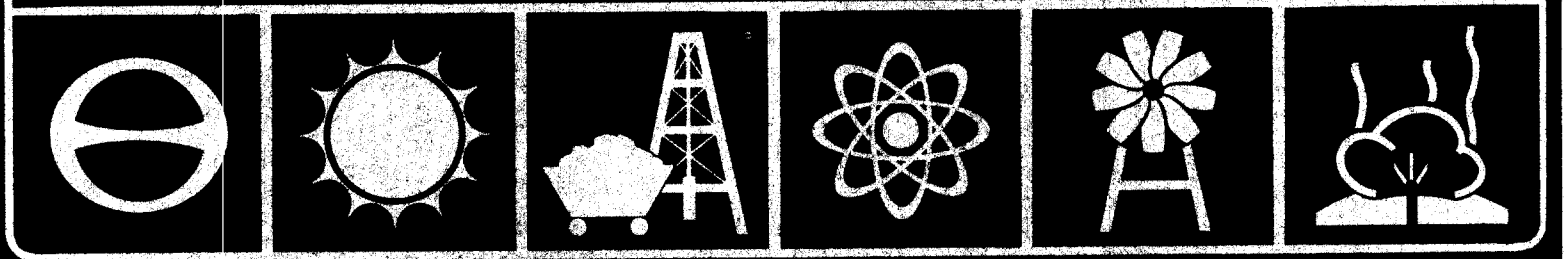

SF 2900-QQB(3-74)

Issued by Sandia Laboratories, operated for the United States Energy Research & Development Administration by Sandia Corporation.

NOTICE

Printed in the United States of America

Available from
National Technical Information Service
U. S. Department of Commerce
5285 Port Royal Road
Springfield, VA 22161

Price: Printed Copy **$4.50**; Microfiche $3.00

Distribution
Category UC-60

SAND76-0130
Unlimited Release
Printed May 1976
Reprinted March 1977

WIND TUNNEL PERFORMANCE DATA FOR THE DARRIEUS WIND TURBINE WITH NACA 0012 BLADES

Bennie F. Blackwell, Robert E. Sheldahl
Aerothermodynamics Division, 1333

Louis V. Feltz
Mechanical Design Division, 1324

Sandia Laboratories
Albuquerque, NM 87115

ABSTRACT

Five blade configurations of a 2-metre-diameter Darrieus wind turbine have been tested in the LTV Aerospace Corporation 4.6- x 6.1-m (15- x 20-ft) Low Speed Wind Tunnel. Rotor solidity, Reynolds number, and freestream velocities tested were in the following ranges:

Solidity:	13%-30%
Reynolds number:	$1\text{-}3 \times 10^5$
Freestream velocity:	7-11 m/s

The airfoil section for all configurations was NACA 0012.

The parameters measured were torque, rotational speed, and tunnel conditions. Data are presented in the form of power coefficient as a function of tip-speed ratio for the various solidities, Reynolds number, and freestream velocities tested.

CONTENTS

FIGURES

FIGURES (cont.)

NOMENCLATURE

A_s	Turbine swept area
c	Blade chord
C	Wind tunnel cross-sectional area
C_D	Drag coefficient
C_P	Power coefficient, $\frac{Q\omega}{1/2\rho_\infty V_\infty^3 A_s}$
C_Q	Torque coefficient, $\frac{Q}{1/2\rho_\infty V_\infty^3 R A_s}$
L	Blade length
N	No. of blades
P	Pressure
P_∞	Freestream static pressure
P_{bar}	Barometric pressure
P_g	Gage pressure in tunnel
Q	Turbine torque
Q_f	Friction tare torque
q_∞	Freestream dynamic pressure, $1/2\rho_\infty V_\infty^2$
R	Turbine maximum radius
Re_∞	Reynolds number per unit length, $\frac{\rho_\infty V_\infty}{\mu_\infty}$
Re_c	Chord Reynolds number, $\frac{\rho_\infty R\omega c}{\mu_\infty}$
T_∞	Temperature

V_∞	Freestream velocity, $V_{\infty_u} (1 + \epsilon_t)$
X_∞	Turbine tip-speed ratio, $\frac{R\omega}{V_\infty}$
δ	Uncertainty
ϵ	Wind tunnel blockage factor
μ_∞	Freestream viscosity
ρ_∞	Freestream density
ω	Turbine rotational speed
σ	Solidity, $\frac{NcL}{A_S}$

Subscripts

u	Uncorrected for blockage
wb	Wake blockage
sb	Solid blockage
t	Total blockage

SUMMARY

Five blade configurations of a 2-metre-diameter Darrieus wind turbine have been tested in the LTV Aerospace Corporation 4.6- x 6.1-m (15- x 20-ft) Low Speed Wind Tunnel. Rotor solidity, Reynolds number, and freestream velocities tested were in the following ranges:

Solidity:	13%-30%
Reynolds number:	$1\text{-}3 \times 10^5$
Freestream velocity:	7-11 m/s

The airfoil section for all configurations was NACA 0012. Two different test modes were employed: constant turbine rotational speed with variable tunnel speed and constant tunnel speed with variable turbine rotational speed. Data are presented in the form of power coefficient as a function of tip-speed ratio for each of the various configurations investigated.

The maximum power coefficient of all configurations tested was found to be approximately 0.35. Increasing Reynolds number increases the power coefficient at all tip-speed ratios for all configurations. Decreasing rotor solidity increases the tip-speed ratio range of operation for which useful power is produced. In order to maximize the peak power coefficient for a given Reynolds number, a solidity in the range of 0.2 to 0.25 should be chosen. The tip-speed ratio for the runaway condition increases for decreasing solidity and/or increasing Reynolds number and windspeed. Two- and three-bladed configurations were tested at the same solidity and Reynolds number; from the standpoint of aerodynamic performance, three blades are slightly better than two. In the design of a starter system for a Darrieus turbine, system friction as opposed to aerodynamic drag may dictate the characteristics of the starter system at low tip-speed ratios. This was definitely true for the small-scale wind tunnel model of this study.

Selected results from an uncertainty analysis are presented in the appendix.

I. INTRODUCTION

The "energy crisis" has forced a new look at an ancient source of energy—the wind. Although the wind was one of the first energy sources that man harnessed, it has been replaced over the years by various technological innovations. James Watt's steam engine, invented in the late 1700's, hastened the demise of the European grain-grinding windmill. Wind energy experienced a brief resurgence in the early 20th century after the Danes demonstrated the feasibility of wind-driven electric generation. However, in Europe the internal combustion engine had lower initial costs and produced cheaper power than the combined wind generator/battery installation. In the United States the downfall of farm-sized wind-driven electrical generators can be attributed to the Rural Electrification Association and other artificially cheap sources of electricity.

The Wind Energy Conversion Branch of the Energy Research and Development Administration (ERDA) has the responsibility of formulating and directing the research and development activities of the Federal Wind Energy Program for the United States. The general objective of this ERDA program is to advance the technology and accelerate the development and utilization of reliable and economically viable wind energy systems. One element of the program is the investigation of innovative wind energy concepts which might provide a significant improvement in performance per unit cost as compared with more conventional wind energy systems. Under sponsorship of the ERDA Wind Energy Program, Sandia Laboratories has been investigating the Darrieus wind turbine as an alternative to the conventional horizontal-axis wind turbine.

The Darrieus turbine was invented by G. J. M. Darrieus of France; patent applications were filed in France and in the United States in 1925 and 1926, respectively. It appears that the Darrieus turbine concept lay dormant until the mid-1960's, when it was independently re-invented by the National Aeronautical Eltablishment of the National Research Council of Canada (NAE/NRC). The previously published experimental data on the aerodynamic performance of the Darrieus turbine

are contained in a series of NAE/NRC reports.[1-4] In order to verify some of the NRC findings, to expand the range of some of the pertinent parameters, and to provide a comprehensive data base for the development of computer models for the prediction of aerodynamic performance, Sandia Laboratories undertook an extensive wind tunnel test program. The purpose of this report is to summarize the primary results from the Darrieus turbine wind tunnel test series conducted at the Vought Corporation, Vought Systems Division 4.6- x 6.1-m (15- x 20-ft) Low Speed Wind Tunnel.

II. TEST MODELS AND INSTRUMENTATION

Two configurations of the 2-metre-diameter wind turbine model are shown installed in the test section in Figures 1 and 2. The turbine consists of the rotating components (tower and blades) held by bearings in the upper collar and in the lower support structure. The upper collar is restrained by steel cables which have a predetermined tension and are affixed to the walls of the test section. The lower support structure is mounted to the I-beams shown on the floor of the tunnel.*

The rotating tower is attached to the power and instrumentation train, shown in Figure 3, which consists of a precision torque and rotation transducer, a right-angle gear transmission with a two-to-one gear ratio, and a speed-controlled 5-hp electric motor. Also included are several shaft flexible couplings.

The blades were machined from a high-strength aluminum alloy (7075-T6) to the required NACA 0012 airfoil shape as a flat ribbon and then formed to the straight-line/circular-arc configuration shown in Figure 4. This shape is an economic compromise to the ideal troposkien (bending stress-free) shape. The details of the troposkien geometry can be found in References 5-7. The blades were inspected for accuracy of geometry after fabrication and were found to be within the demanded rigid specifications.

Since the test matrix included several blade solidities (chords), it was necessary to provide a means of alternating the blade sets on the tower. The method selected consisted of a double-wedged foot (with a half-angle of about two and one-half degrees) machined integrally on both ends of the blade. The hubs at each extremity of the tower included matching wedge surfaces with removable plates at the inner surfaces. It was required to have both a two-bladed and a three-bladed

---

* These heavy I-beams are required for locating the turbine in the center of the test section while avoiding damage to the moving ground plane apparatus located on the tunnel floor at this location.

tower constructed in the above manner. The towers themselves were of solid steel rod in a lattice structure geometrically scaled from towers considered representative of full-size wind turbines.

The seemingly extravagant wedge method of mounting the blades is necessary because the blade centrifugal (tensile) stresses are highest at the blade location where the juncture with the tower must be made. This prevents incorporation in the blade ends of holes, steps, or other—more conventional—design approaches which include unacceptable stress concentration factors.

The method selected permits blade changes to be made in the wind tunnel in less than one-half hour. Entire tower/blade changes require about 1 hour. Thus, the added fabrication costs were offset by the tunnel occupancy cost reductions effected by these quick changes.

The bearing arrangement included one double-row type of self-aligning ball bearing at the lower location and a set of two single-row radial contact ball bearings in the upper collar. Because of the importance of precise determination of torques, bearing selection and loading are critical. Turbine torque and rotational speed were measured through a LeBow Torque Sensor Model 1404-200* and its associated signal conditioning equipment. This device incorporates a two-channel (from strain gage bridge legs) rotary transformer to extract the bridge signal from the rotating shaft without mechanical contact. The bridge signal is indicative of the torque, which is proportional to the shaft windup. The device is closely compensated for temperature variation and is advertised as having a nonlinearity of only ±0.1 percent of full scale.

The "full-scale" recommended torque of the device selected was 200 pound-inches but, because overloading is allowed, the transducer was calibrated to 300 pound-inches. The alternate approach of selecting a transducer rated at an initially higher "full scale" (the next increment was 500 pound-inches) would have seriously degraded the torque resolution in the lower ranges and in the determination of the

---

*Lebow Associates, 1728 Maple Lawn Road, Troy, Michigan 48084

tare torques of the turbine. The transducer was shaft mounted between the turbine and the gear box and was restrained from case rotation by glass-fiber tape straps attached to the lower structure to minimize mechanical noise input to the transducer. The transducer performed exceptionally well, even in the "overrated" application, and, except for a shortcoming in mechanically protecting a transformer component, the entire system design is considered to be superior for this application.

The torque transducer is mechanically coupled to the electric motor by a right-angle spiral bevel gear box, which permits two revolutions of the electric motor for every revolution of the turbine. This permits the electric motor to operate on a more optimum portion of its power vs rpm curve than in utilizing a direct (one-to-one) coupling to the turbine.

A 3-phase, 440-volt controlled-speed electric motor system was considered superior to competing turbine loading systems in that it could fix the turbine rpm at a desired constant value in the unstable region, which occurs from the "starting" threshold to the peak of the turbine torque curves. In addition to a standard Morse VLT-5 AC adjustable speed controller, a load bank (of varying wattage light bulbs) was also included to permit the motor to act as a generator absorbing the power produced by the turbine. The system was designed so that the speed controller continued to function, even when the turbine-produced energy caused the motor to act as a generator. This speed control is maintained until "breakaway" torque is exceeded. With the inclusion of the two-to-one gear box, however, breakaway did not occur during the entire test series. The velocity extremes set forth in the text matrix can cause load-matching problems in the controlled-speed motor system unless considerable attention is given to the design, adjustment, and operation of this system.

Figure 5 is a schematic of the turbine, instrumentation, and load system.

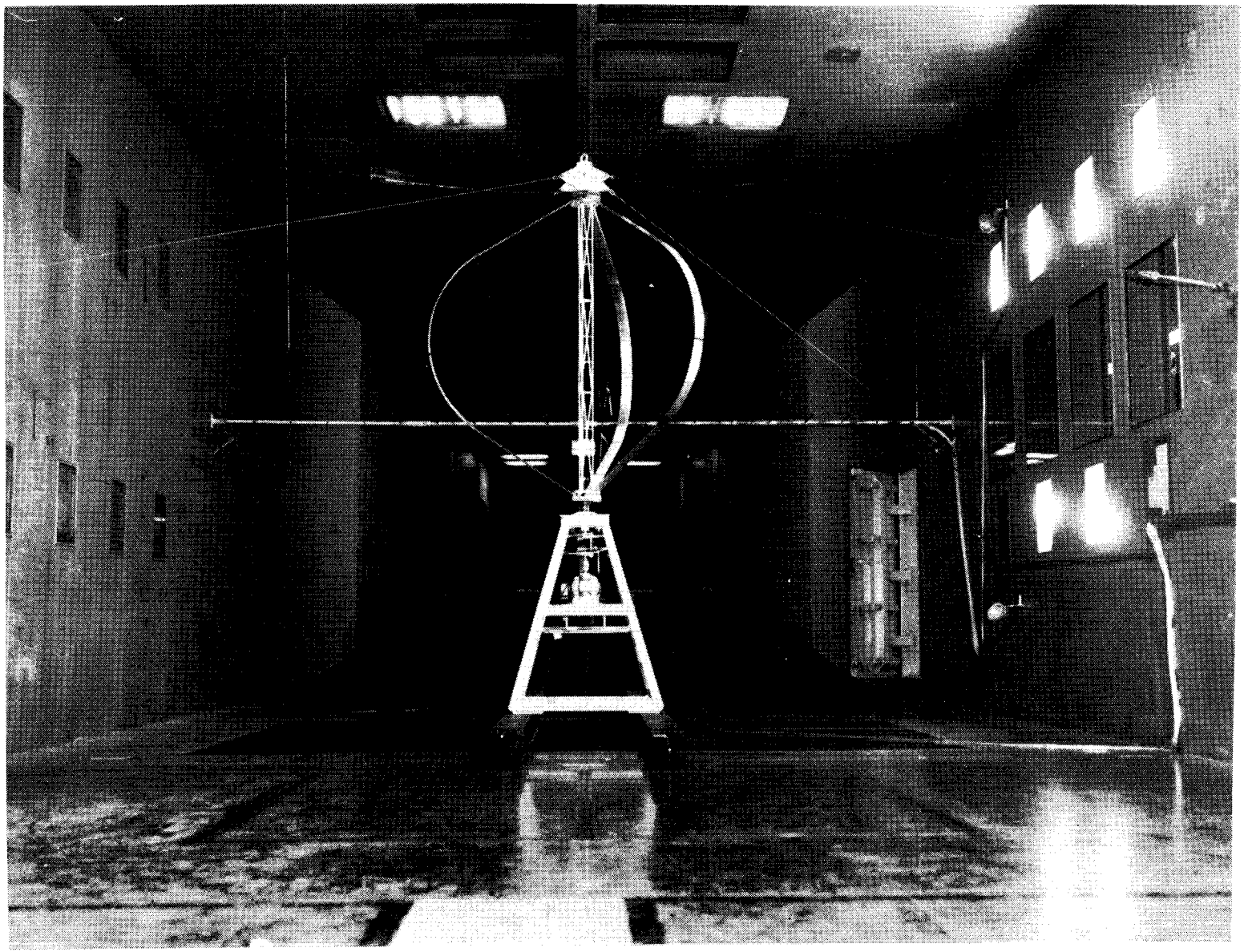

Figure 1. Three-Bladed Darrieus Wind Turbine Model in the Vought Systems Division 15- x 20-Foot Low Speed Wind Tunnel (looking downstream)

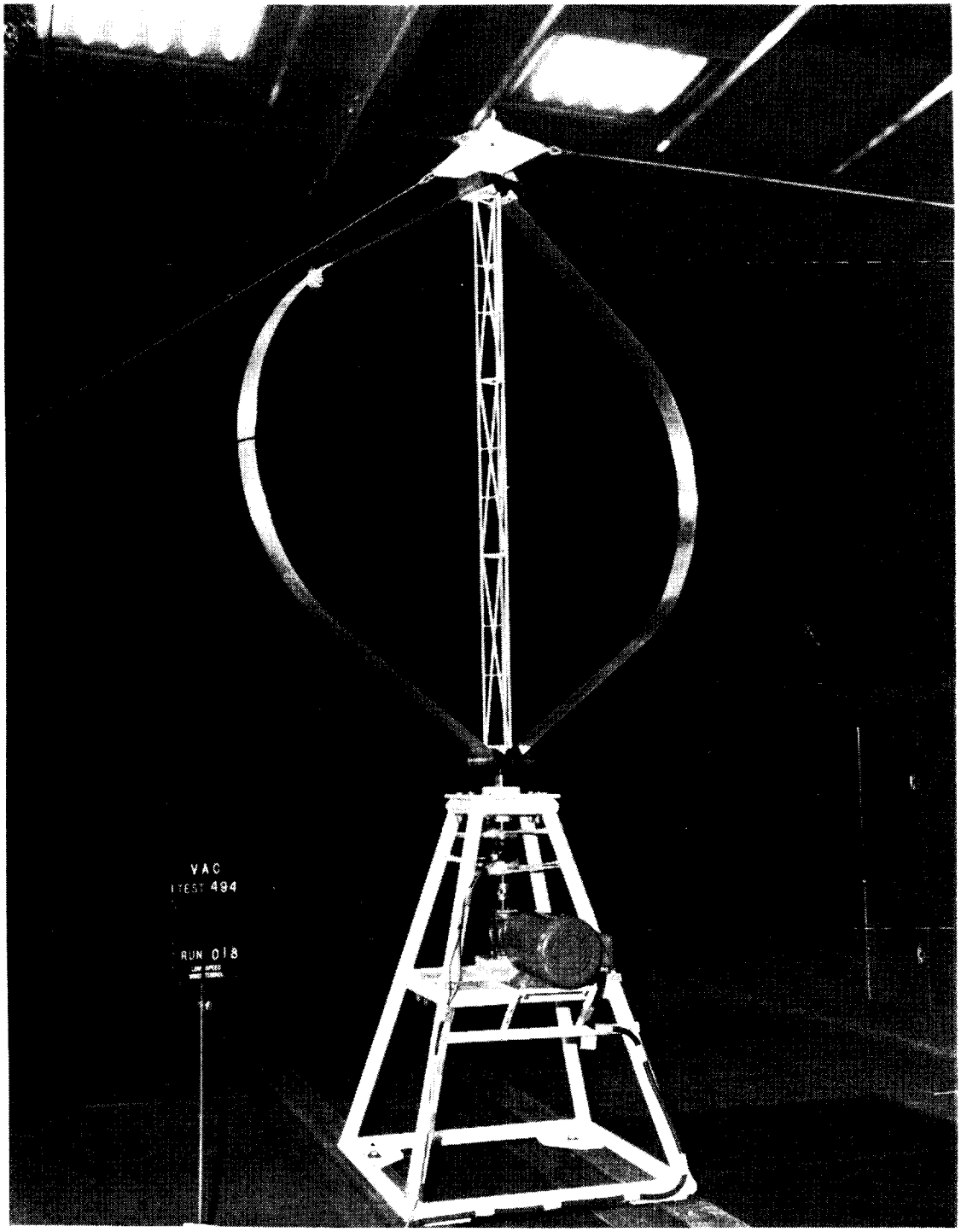

Figure 2. Two-Bladed Darrieus Wind Turbine Model

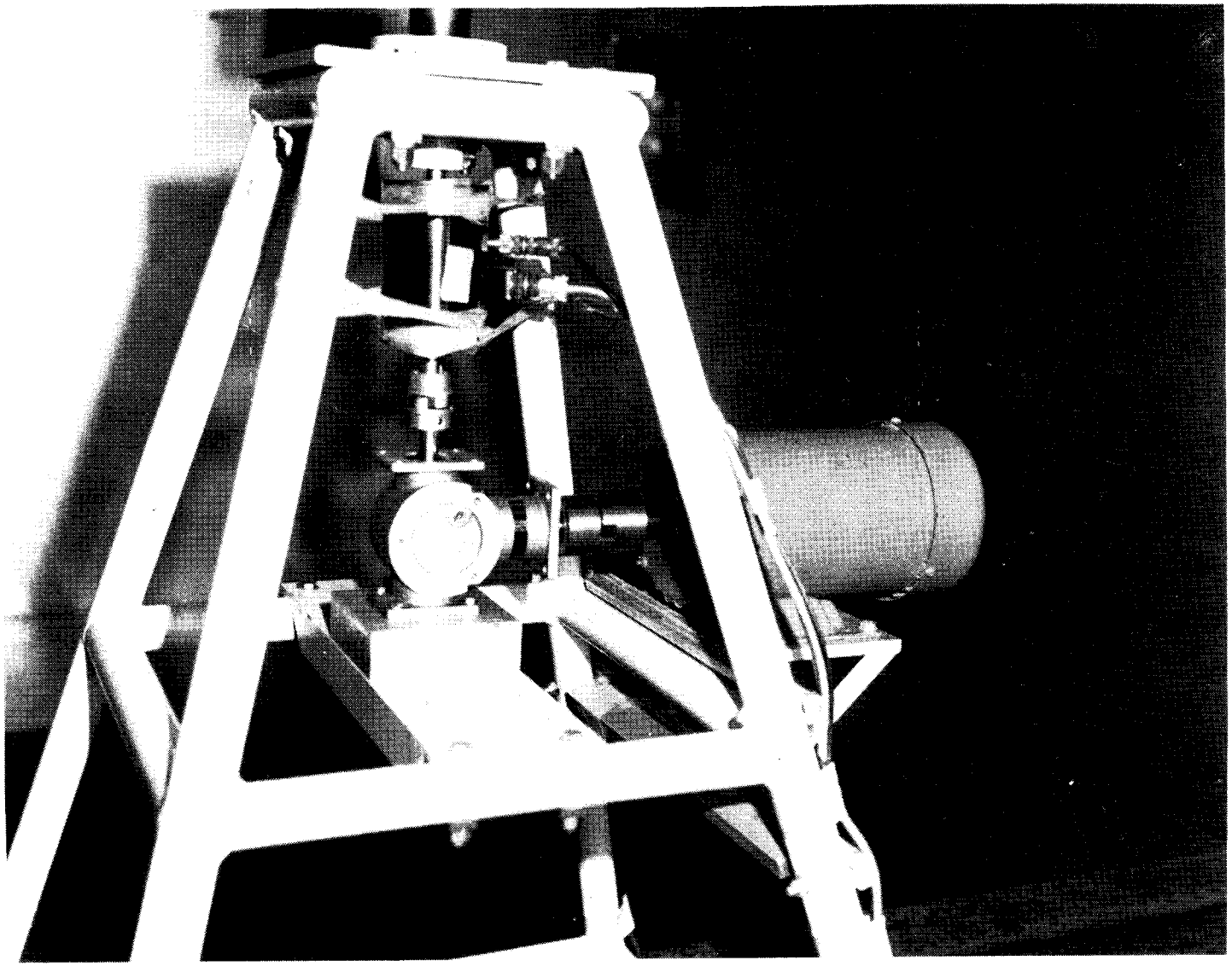

Figure 3. Torque Transducer, Couplings, Right-Angle Gear Box, and Electric Motor/Generator

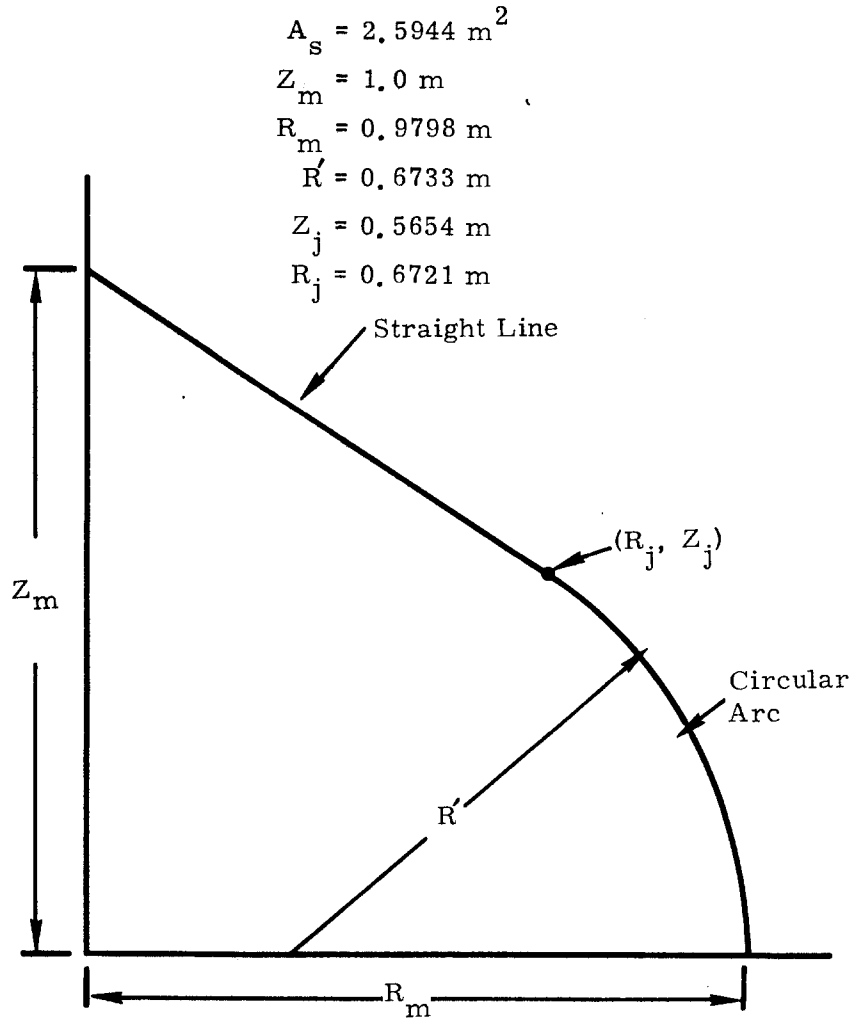

Figure 4. Geometry of Wind Tunnel Test Blade (straight-line circular-arc approximation to troposkien)

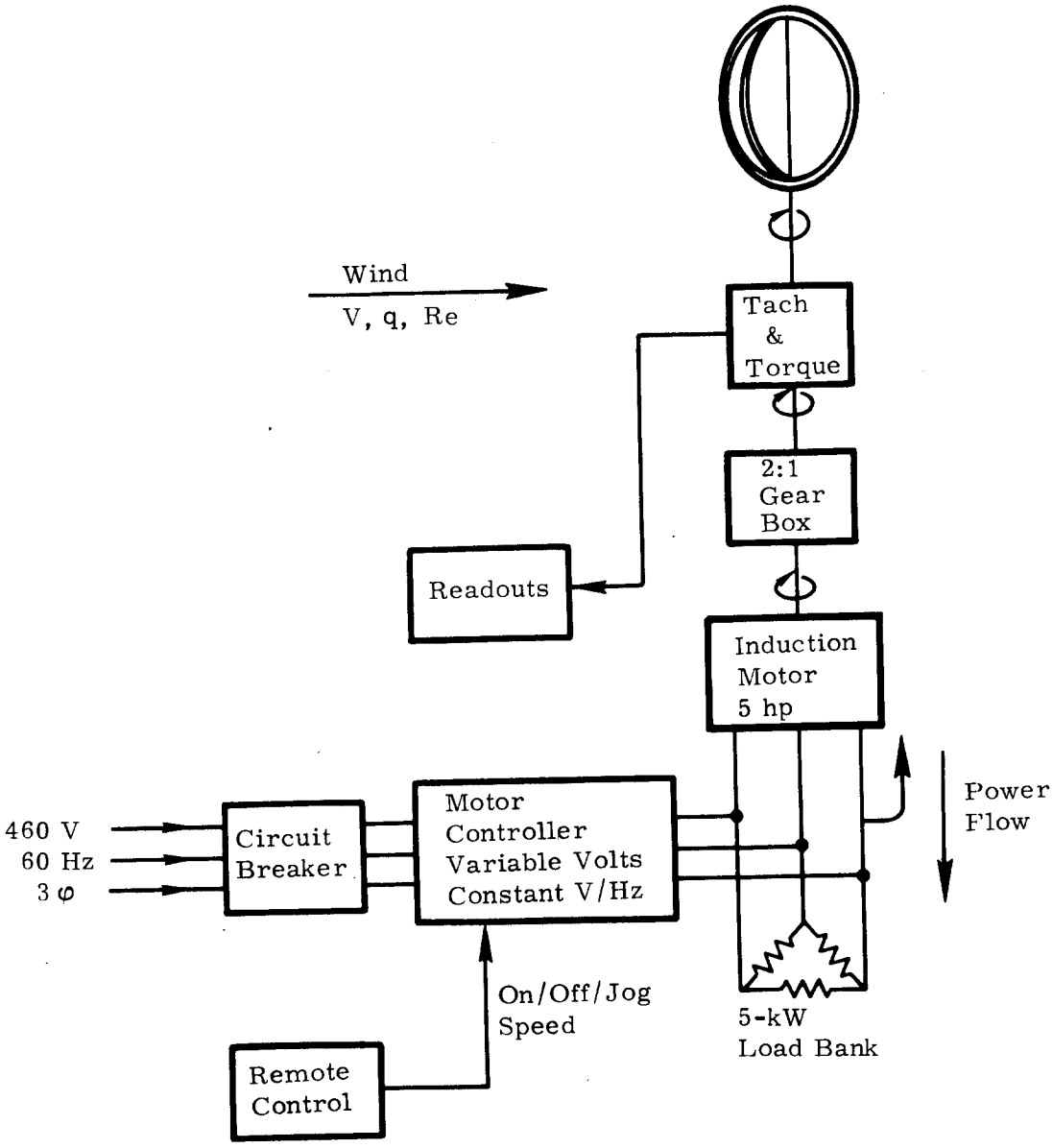

Figure 5. Schematic of Wind Turbine/Instrumentation/Load System

III. TEST FACILITY

The Vought Systems Division Low Speed Wind Tunnel[8] is a horizontal single-return, tandem test section, closed-circuit facility. The facility contains a rectangular 2.1- x 3.0-m (7- x 10-foot) test section with a rectangular 4.6- x 6.1-m (15- x 20-foot) test section 11.9 metres long located upstream of the 2.1- x 3.0-m section. This section has a windspeed range of 3 to 23 m/s. Because of its size and speed range, it was chosen as the facility to test the wind turbine models. Figure 1 shows the wind turbine in the 15- x 20-foot section. The photograph was taken looking downstream into the contraction section of the 7- x 10-foot test section. The wind tunnel control room is located behind the windows shown on the right side of the photograph. The wind turbine instrumentation and the controls for the operation of the wind turbine, as well as the facility controls, were operated from that station. The windows permitted visual observation of the turbine and also allowed video and camera coverage.

All instrumentation pertaining to the operation of the facility and wind tunnel flow conditions were provided by Vought. Sandia provided the instrumentation associated with obtaining turbine torque, Q, and turbine rotational speed, ω. The torque and turbine speed data were recorded by Vought along with their data for dynamic pressure, q_∞, static temperature T_∞, static pressure P_∞, and wind velocity, V_∞. The data were recorded on punched cards for later computer data reduction.

IV. TEST PROCEDURE

Two types of tests were performed with the Darrieus turbine. One type was with a constant wind velocity where the turbine rotational speed was varied over a tip-speed ratio from approximately unity to turbine runaway. Runaway is the high-speed condition where the output torque is equal to the friction torque of the system and no power is produced. The second type of test consisted of operating the turbine at a fixed rotational speed and varying the wind velocity to span the range of tip-speed ratios from 2 to runaway. The second mode of testing was included because that would best simulate the synchronous operation of an actual system[9] and it also would give a more realistic Reynolds number effect on the blade performance. The actual wind velocity the blades see is a greater function of the turbine rotational speed than the freestream air velocity, since the tip speed is several times the wind-speed (the tip-speed ratio range of operation may be 2-10). The test matrix for the wind turbine tests is shown in Table I.

The tension of the support cables from the tunnel walls to the top of the turbine, as seen in Figure 1, was monitored by load cells at all times and was maintained at a constant level for all the tests. These functions were performed to maintain a constant load on the tower bearings.

Before the blades were installed on the turbine tower, the tower was rotated by the motor and the tare torque for various speeds was obtained. This value was very consistent over the rotational speed range and was considered to be caused primarily by the friction in the bearings. This value of tare torque was recorded for each configuration.

For the constant wind velocity tests, the wind tunnel was stabilized at the prescribed operating condition and held at that condition for the duration of the test. The turbine was then started with the electric motor and controller and brought to a specified rotational speed, usually starting at a low-tip-speed ratio. A data point was taken, and the turbine rotational speed was then increased by changing the

TABLE I

Darrieus Rotor Tests in the Vought Systems Division

Low Speed Wind Tunnel

Run No.	Configuration Number	No. of Blades	Solidity (%)	Rotor Speed (rpm)	Wind Velocity (m/s)	Chord (cm)	Chord Reynolds Number
1	1	3	30	180	Variable	8.815	104,000
2	1	3	30	267	Variable	8.815	150,000
3	1	3	30	500	Variable	8.815	290,000
5	1	3	30	Variable	11	8.815	Variable
6	1	3	30	Variable	9	8.815	Variable
7	2	3	25	216	Variable	7.346	101,000
8	2	3	25	320	Variable	7.346	151,000
9	2	3	25	600	Variable	7.346	278,000
10	2	3	25	Variable	11	7.346	Variable
11	2	3	25	Variable	9	7.346	Variable
13	3	3	20	270	Variable	5.877	101,000
14	3	3	20	400	Variable	5.877	154,000
15	3	3	20	525	Variable	5.877	200,000
16	3	3	20	Variable	9	5.877	Variable
17	3	3	20	Variable	7	5.877	Variable
18	4	2	20	180	Variable	8.815	106,000
19	4	2	20	267	Variable	8.815	156,000
20	4	2	20	350	Variable	8.815	204,000
21	4	2	20	500	Variable	8.815	290,000
22	4	2	20	Variable	9	8.815	Variable
23	4	2	20	Variable	11	8.815	Variable
24	5	2	13	Variable	7	5.877	104,000
25	5	2	13	270	Variable	5.877	155,000
26	5	2	13	400	Variable	5.877	200,000
27	5	2	13	525	Variable	5.877	Variable
28	5	2	13	Variable	9	5.877	Variable

$A_s = 2.5944\ m^2$

$R = 0.9798\ m$

controller setting. The tip-speed ratio was increased in increments of approximately 0.25, and a data point was taken at each step when the turbine speed had stabilized. This process continued until the tip-speed ratio exceeded the runaway condition.

The constant rotational speed (constant Reynolds number) tests were performed by operating the wind turbine at a constant rpm for the duration of the test. The wind tunnel was then set at a given operating condition, usually starting with a low wind velocity, and allowed to stabilize. Once the facility was operating stably, a data point was taken. The facility windspeed was then increased to the next operating point and allowed to stabilize for the next data point. This process was continued in increments of tip-speed ratios of approximately 0.25.

V. DATA REDUCTION

The wind tunnel turbulence factor for the 15- x 20-foot section is quite high:[8] 1.4 at a velocity of 20 m/s. Because this turbulence factor is determined by a stationary turbulence sphere and the wind turbine blades are moving at a speed greater than the windspeed, the use of a turbulence factor to correct to an effective Reynolds number was not attempted. Repeating: no Reynolds numbers stated in this report are corrected for the wind tunnel turbulence factor.

When an object is placed in a wind tunnel, the object produces some "tunnel blockage," which causes an increase in the wind velocity in the test section. This increase has to be accounted for by the determination of a tunnel blockage factor, ϵ, sometimes called the velocity increment. The total factor is the sum of the velocity increment caused by wake blockage and solid blockage.

$$\epsilon_t = \epsilon_{wb} + \epsilon_{sb} \,, \tag{1}$$

where

$$\epsilon_{wb} = \frac{\Delta V}{V_{\infty_u}} = \frac{A_s}{4C} C_{D_u} \tag{2}$$

$$\epsilon_{sb}\,(\text{Blades}) \cong 0 \tag{3}$$

$$\epsilon_{sb}\,(\text{STAND}) \cong \frac{\text{Stand Frontal Area}}{4C} \,. \tag{4}$$

The above relationships can be found in Pope and Harper.[10] Templin[4] shows that the drag coefficient for a Darrieus wind turbine is a function of the tip-speed ratio and theoretically goes to 1.0. A drag coefficient of 1.0 was chosen as the uncorrected drag coefficient to apply for all tip-speed ratios. The tunnel blockage factor

was anticipated to be small, and the accuracy of assuming a constant drag coefficient was thought to be within the accuracy of the correction. The calculated wake blockage for the turbine (Eg. (2)) is 0.023 and the calculated solid blockage for the stand and hardware is 0.003 for a total blockage factor, ϵ_t, value of 0.026. This factor is used to correct the freestream velocity and dynamic pressure as shown.

$$V_\infty = V_{\infty_u} (1 + \epsilon_t) \tag{5}$$

$$q_\infty = q_{\infty_u} (1 + 2\epsilon_t) \tag{6}$$

The data taken by Vought consisted of: q_∞, ω, P_∞, T_∞. These data are punched on cards and entered into the computer. The freestream density, ρ_∞, is calculated by using the equation of state with the measured values of P_∞ and T_∞. Knowing ρ_∞, one can determine the freestream velocity by

$$V_\infty = \sqrt{\frac{2q_\infty}{\rho_\infty}} \quad , \tag{7}$$

where q_∞ has been corrected for the blockage factor. The Reynolds number per unit length for each test condition is computed by

$$Re_\infty = \frac{\rho_\infty V_\infty}{\mu_\infty} \quad . \tag{8}$$

The blade chord Reynolds number is computed by

$$Re_\infty = \frac{\rho_\infty R\omega c}{\mu_\infty} \quad . \tag{9}$$

The computation of the performance data is as follows:

$$X_\infty = \frac{R\omega}{V_\infty} \tag{10}$$

$$C_Q = \frac{Q + Q_f}{1/2\rho_\infty V_\infty^2 RA_s} \tag{11}$$

$$C_P = \frac{(Q + Q_f)\,\omega}{1/2\rho_\infty V_\infty^3 A_s} \tag{12}$$

The data for torque and power coefficients are plotted as a function of the tip-speed ratio and are corrected for tunnel blockage and tare torque.

VI. TEST RESULTS

The performance characteristics of five different turbine blade configurations were evaluated both for constant turbine rotational speed and for constant tunnel-freestream velocity. The detailed test matrix is presented in Table I. Rotor solidity, which is the ratio of total blade planform area* to rotor swept area,† was the primary variable that changed from one configuration to the next. This solidity change was accomplished by changing the blade chord and/or the number of blades; the rotor swept area and NACA 0012 airfoil section were kept fixed for all configurations. Each configuration was tested over a range of tip-speed ratios, Reynolds numbers, and freestream velocities. The format chosen for presentation of the performance data was power coefficient as a function of tip-speed ratio for the various Reynolds numbers and freestream velocities. Various cross plots are also presented.

Figures 6-10 present the power coefficient data for each of the five configurations tested at constant Reynolds number. As one would expect, increasing the Reynolds number increases the power coefficient for all tip-speed ratios and configurations tested. The tip-speed ratio for zero power (runaway condition) increases with increasing Reynolds number.

The maximum power coefficient achieved by any of the configurations was approximately 0.35. One might be inclined to conclude that the maximum power coefficient for Darrieus-type wind turbines is less than the often-quoted C_p = 0.4-0.45 for high-performance horizontal-axis wind turbines. However, theoretical calculations by Strickland[11] have shown that the maximum C_p is approximately 0.48 for a blade Reynolds number of 3×10^6 and solidity of 30 percent. Therefore, from the standpoint of maximum power coefficient, it is felt that the Darrieus turbine is comparable to the horizontal-axis turbine at comparable Reynolds numbers.

---

*The blade planform area for a constant chord blade is the number of blades times blade chord times blade length.

†A rotating blade of the Darrieus turbine sweeps out a volume which is symmetric about the axis of rotation; this is called the swept volume. The area common to the swept volume and to a plane containing the axis of rotation is called the swept area.

If a wind turbine is to be operated synchronously,[9] the maximum torque point is of considerable importance. (The torque coefficient is defined through the relationship $C_Q = C_P/X_\infty$). The data points corresponding to maximum C_Q are indicated in Figures 6-10 by closed symbols. For the Darrieus turbine, peak C_Q always occurs at a lower tip-speed ratio than does peak C_P. With increasing Reynolds number, the tip-speed ratio corresponding to peak C_Q decreases.

The effect of solidity on the power coefficient is shown in Figures 11 and 12 for Reynolds numbers of approximately 1.5×10^5 and 2.0×10^5, respectively. All five configurations were tested at $Re_c = 1.5 \times 10^5$, but only two at $Re_c = 2.0 \times 10^5$. The most noticeable influence of solidity is that the runaway-condition tip-speed ratio increases with decreasing solidity. For a synchronous application, this implies that power can be produced over a greater windspeed variation for a given turbine rotational speed. The tip-speed ratio at which the power coefficient is a maximum increases with decreasing solidity. If it is desired to maximize the power coefficient, a solidity in the range from 0.2 to 0.25 should be chosen.

The theoretical turbine performance model developed by Strickland[11] indicates that the only influence of the number of blades is through its effect on solidity ($\sigma = NcL/A_s$). It is obvious that a blade in the downwind half of its revolution does not see the same induced velocity field as when in the upwind half of its revolution and that the interference effects should probably be some function of the number of blades. In order to determine the magnitude of this effect, the solidity and Reynolds number were kept fixed while the number of blades was varied. The results of these tests are presented in Figures 13 and 14 for Reynolds numbers of approximately 1.5×10^5 and 2.0×10^5. It appears that the three-bladed configuration is slightly better than the two-bladed configuration. The difference seems to be the most pronounced in the tip-speed ratio range of 3 to 4 and increases with increasing Reynolds number. The peak power coefficient does not appear to be markedly affected by the number of blades for a given solidity. A satisfactory explanation for this behavior has not been found.

Each of the five configurations was also tested at a constant freestream velocity of 9 m/s and of either 7 m/s or 11 m/s. With certain configurations, the 11-m/s tunnel speed would have caused excessive turbine rotational speeds; hence,

this condition was not tested. The basic constant freestream velocity data are presented in Figures 15-19. As one might expect, at a given tip-speed ratio the power coefficient increases with increasing windspeed. This can be visualized by noting that for a constant tip-speed ratio the blade speed (and hence Reynolds number) is directly proportional to the tunnel speed.

For a constant freestream velocity test condition, the blade Reynolds number is directly proportional to the tip-speed ratio. Since some of the data in Figures 15-19 are for a tip-speed ratio range from 1 to 8, there is a Reynolds number variation by a factor of 8. The constant Reynolds number data showed that a change in blade Reynolds number by a factor of 2 could produce a considerable change in the power coefficient data. Consequently, it is felt that any analytical model attempting to predict constant freestream velocity data must be able to handle aerodynamic section data as a function of Reynolds number.

The effect of solidity on the power coefficient data for a constant freestream velocity of 9 m/s is presented in Figure 20. The shape of the power coefficient curve for the constant freestream velocity runs exhibits the same trends with solidity as does the constant Reynolds number data.

Figure 21 compares performance data for two of the Sandia configurations tested at constant freestream velocity with NRC data presented by Templin.[4] The indicated freestream velocity range for the NRC data was 4.7-6.1 m/s; however, the specific rotational- and tunnel-speed combination were not known for the individual data points. The NRC data exhibit a slightly higher peak power coefficient occurring at a higher tip-speed ratio than the Sandia data. Some unexplained discrepancies obviously exist between the two data sets.

It is well known that the Darrieus turbine is not self-starting because the torque coefficient is negative in the tip-speed ratio range of approximately 0 to 2. The relative uncertainty in the performance data in this tip-speed ratio range is high because the torque levels were of the order of 1 percent of full-scale torque. Even though the data uncertainty may be relatively high, the friction-only torque was always very close to the torque measured in the tip-speed ratio range of 0 to 2. This leads one to the very important conclusion that the design of a starter system for a small Darrieus turbine will be dictated by the mechanical friction

in the system and not by the fact that the C_Q curve is negative for X_∞ in the range of 0 to 2. At this time, it is not known whether the same statement will hold true for large-scale systems.

It is not considered necessary to include the raw data in this report, because most readers are interested only in the general results; however, those people attempting to develop prediction models may be interested in the details of the raw data. Consequently, a separate report containing the raw data will be published at a later date and a copy may be obtained directly from the authors.

Selected results from an uncertainty analysis are presented in the appendix.

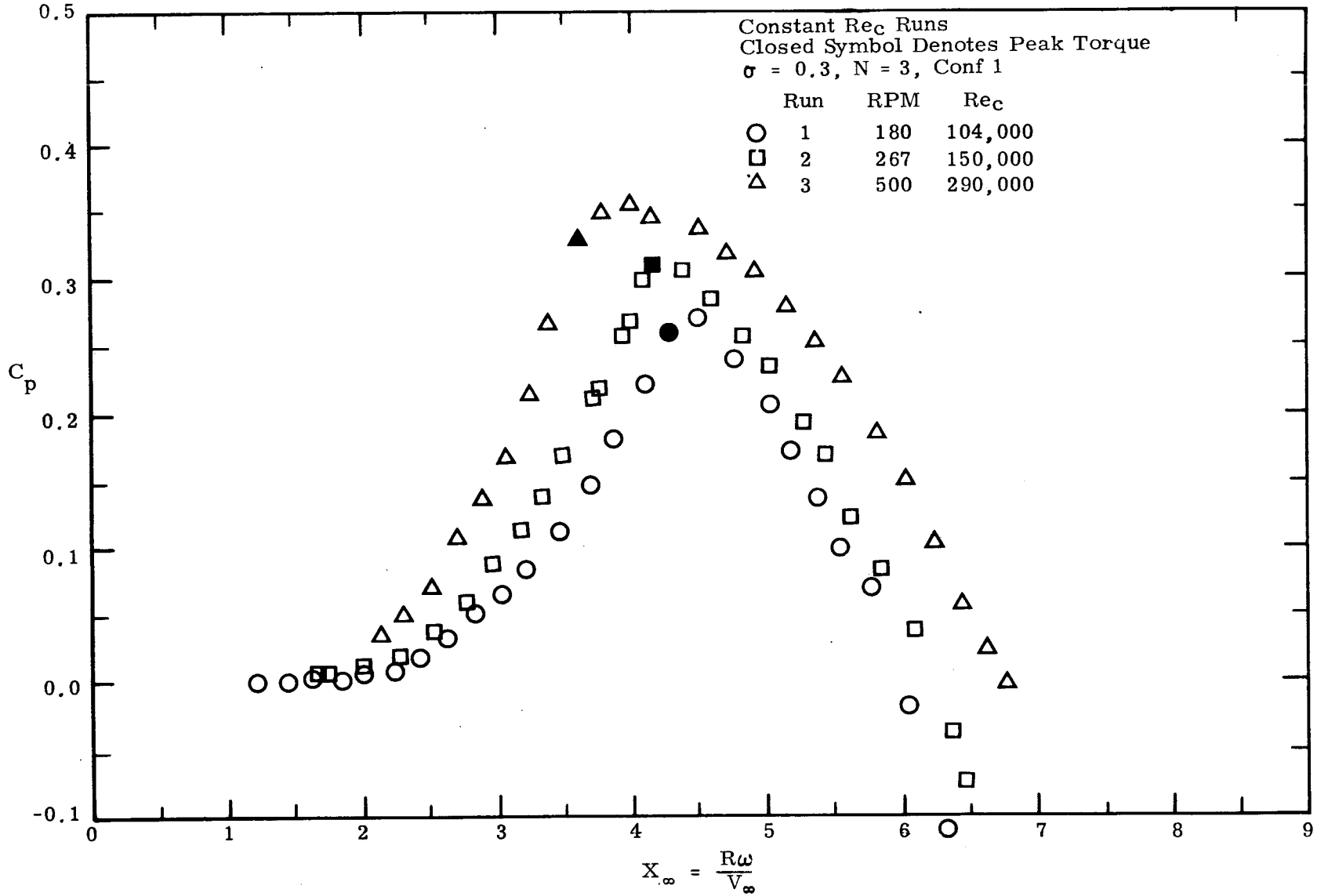

Figure 6. Power Coefficient Data for σ = 0.3, Constant Reynolds Number

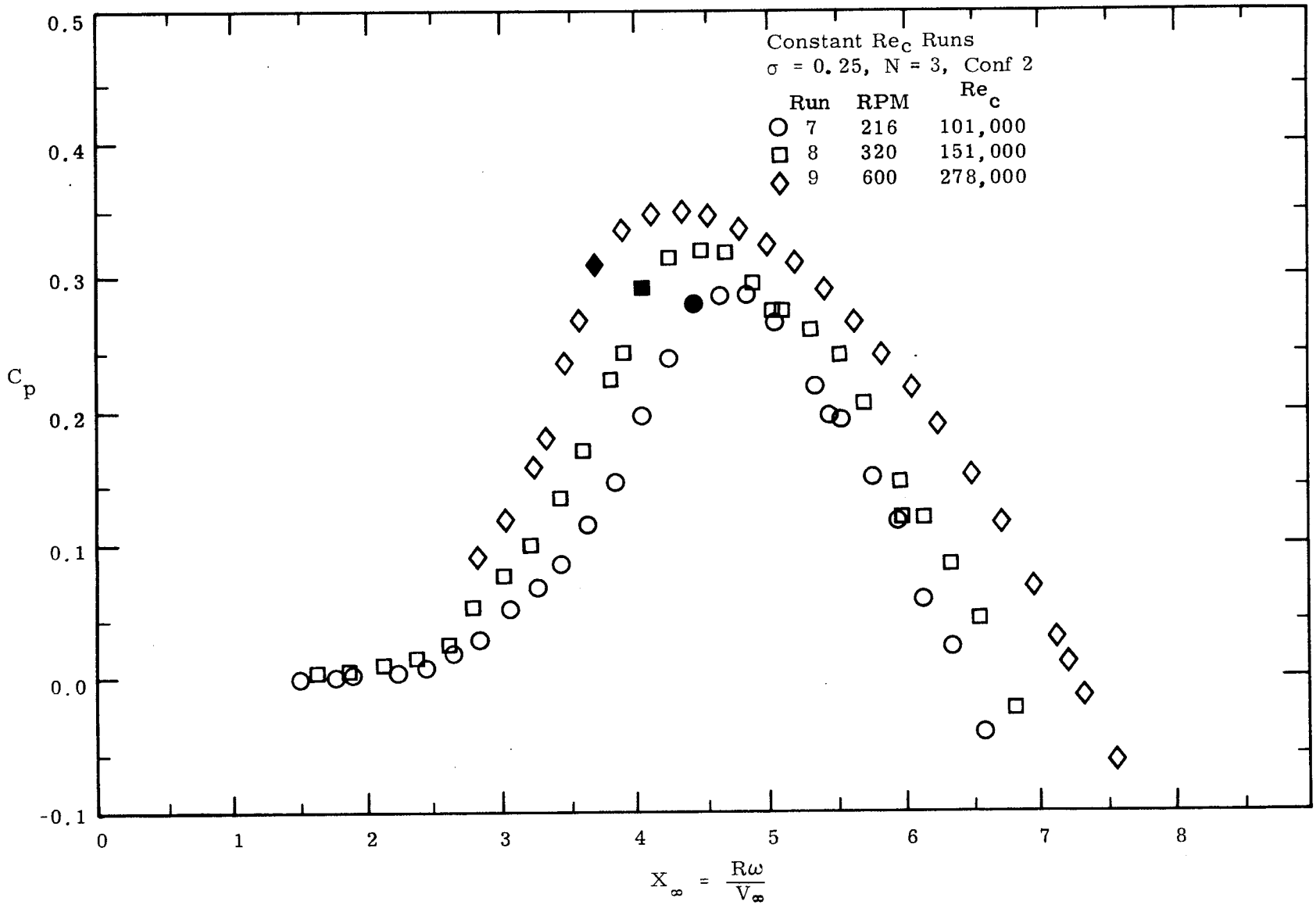

Figure 7. Power Coefficient Data for σ = 0.25, Constant Reynolds Number

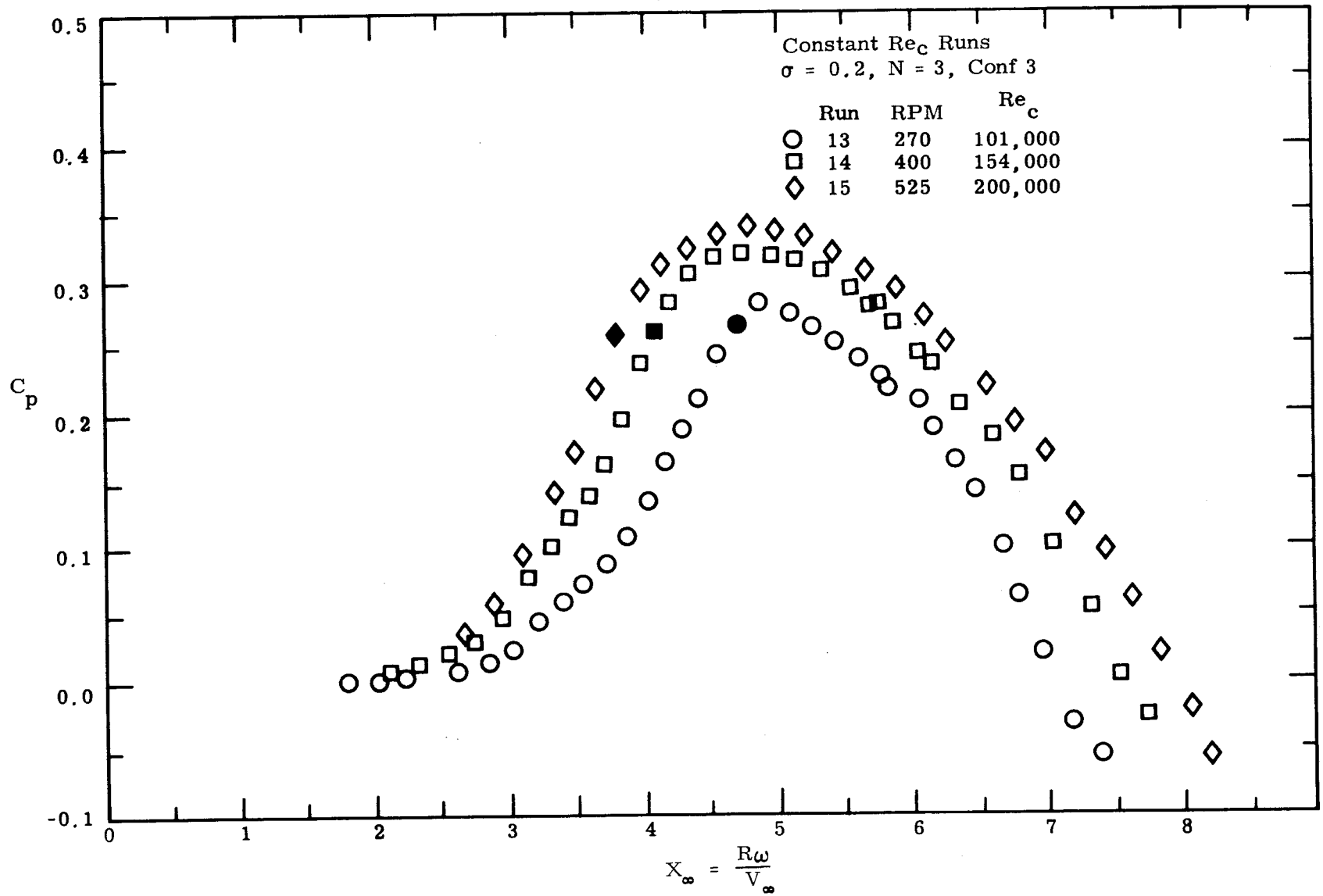

Figure 8. Power Coefficient Data for σ = 0.2, Constant Reynolds Number (N = 3)

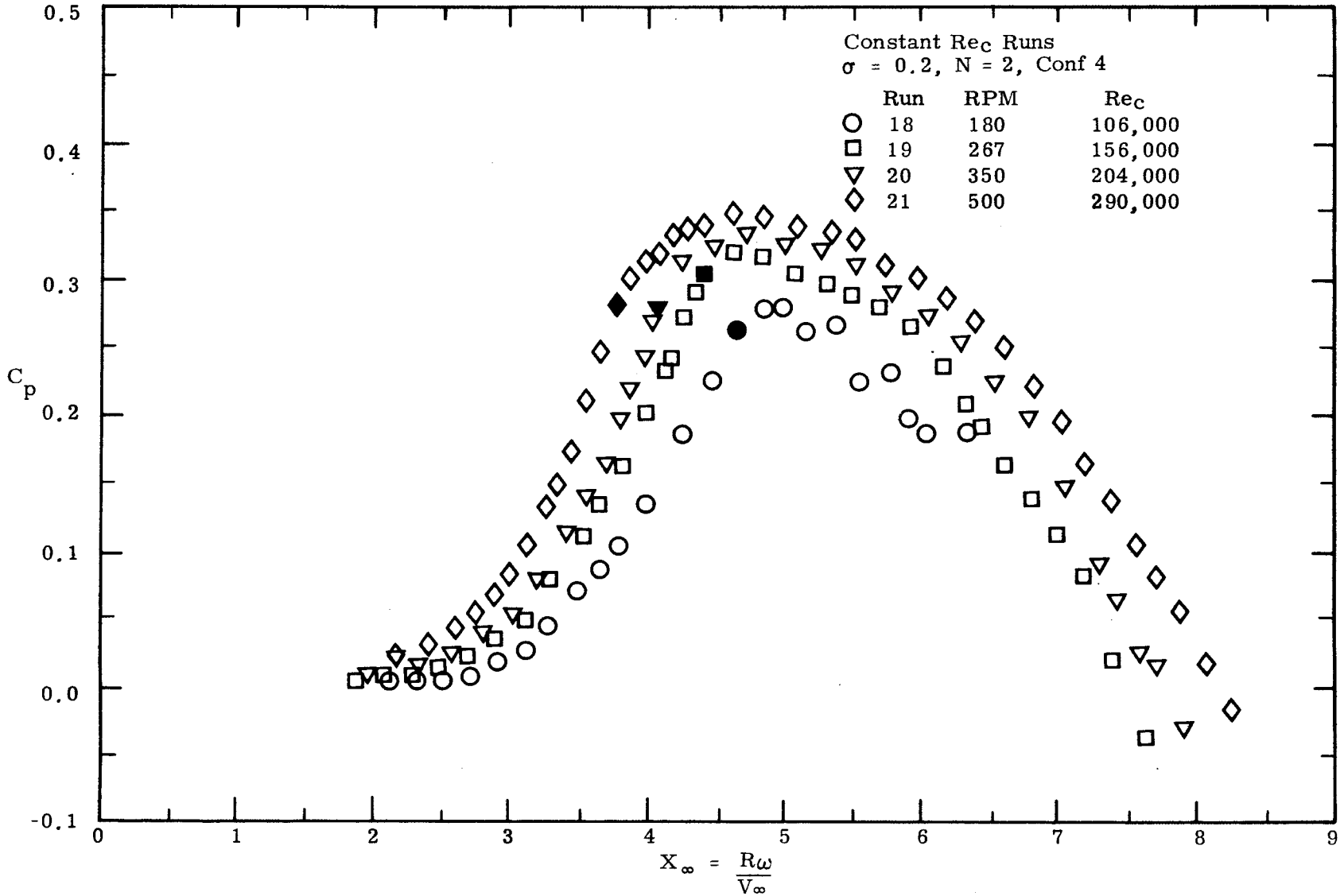

Figure 9. Power Coefficient Data for σ = 0.2, Constant Reynolds Number (N = 2)

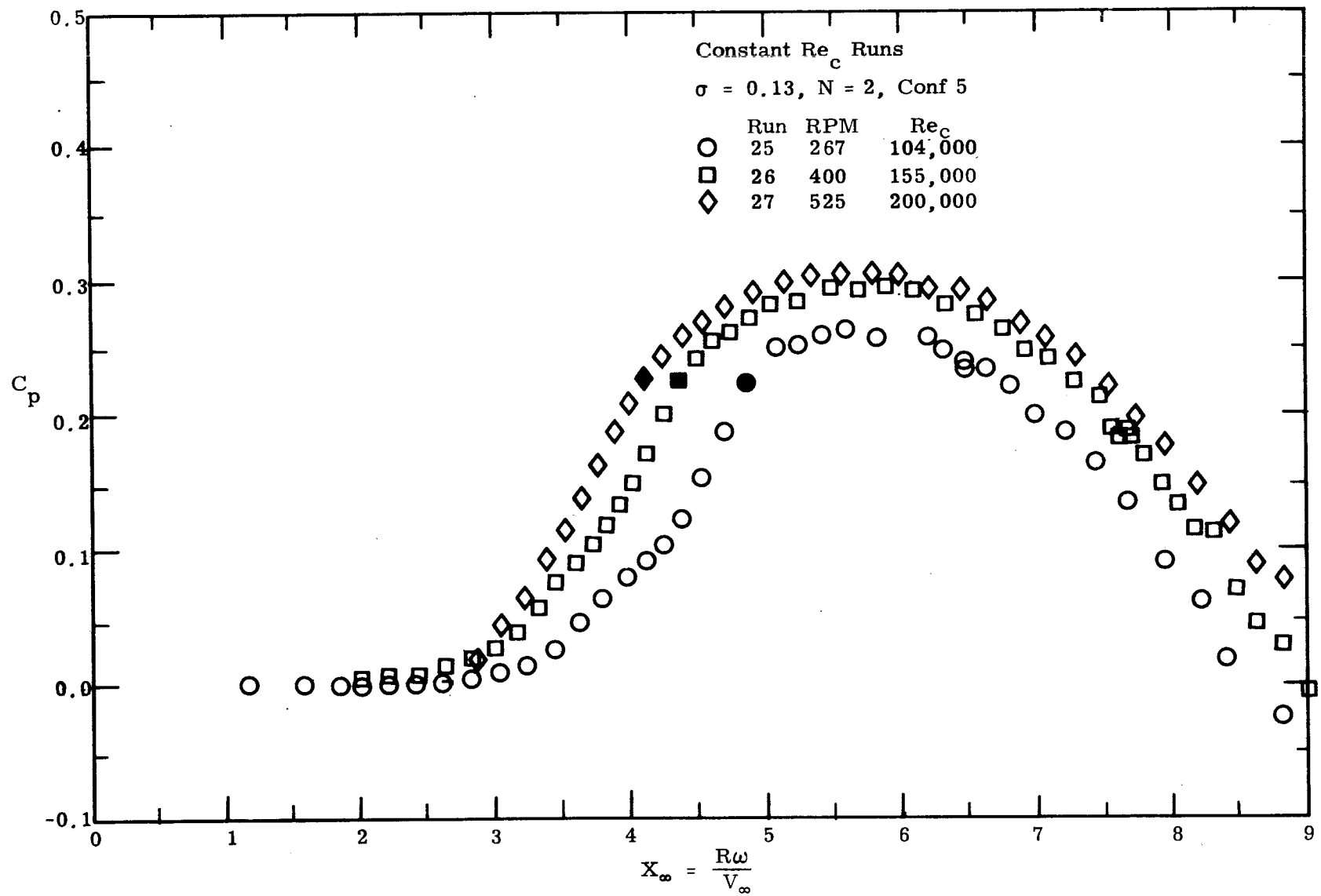

Figure 10. Power Coefficient Data for σ = 0.13, Constant Reynolds Number

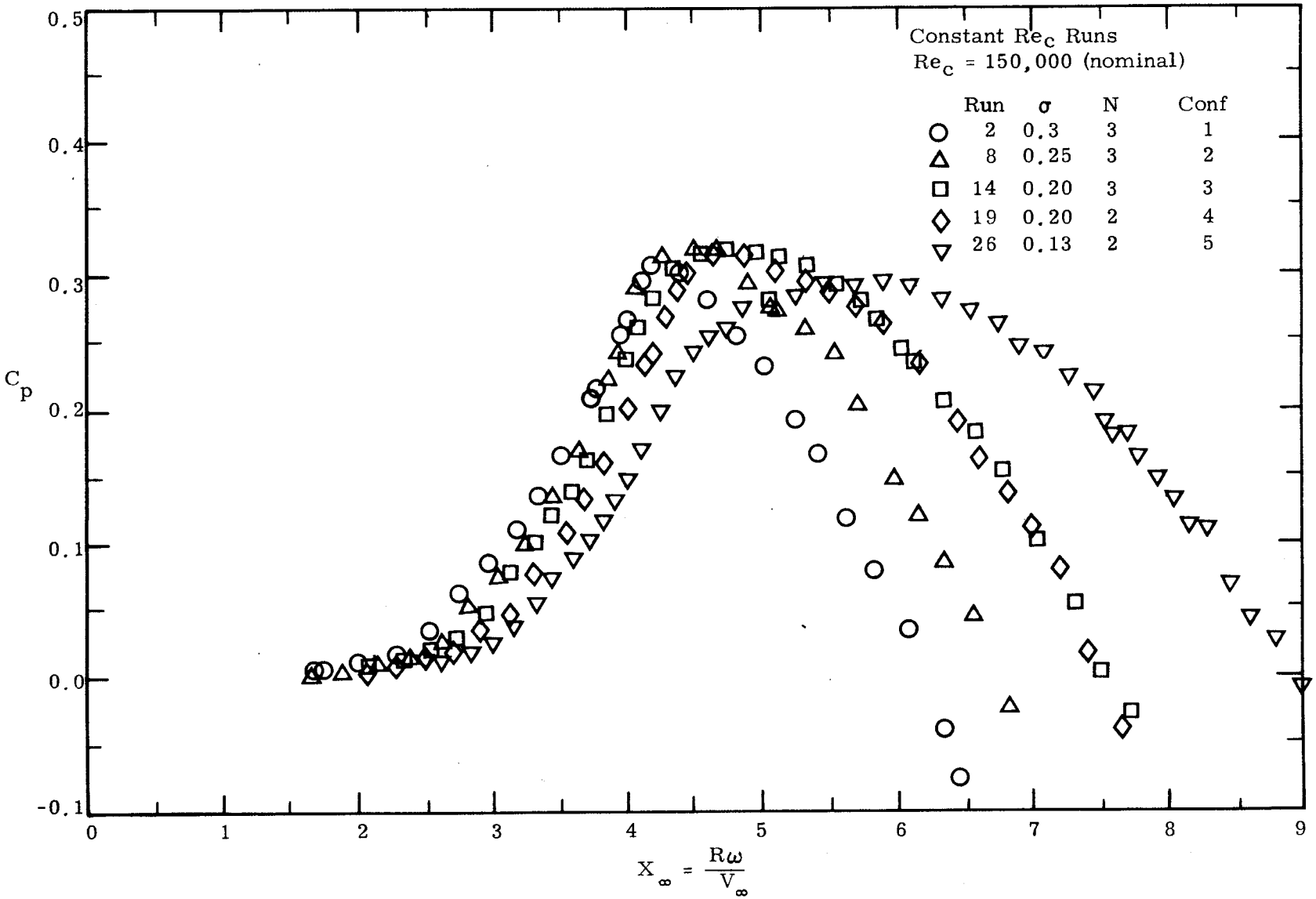

Figure 11. Effect of Solidity on Power Coefficient Data at Re_c = 150,000

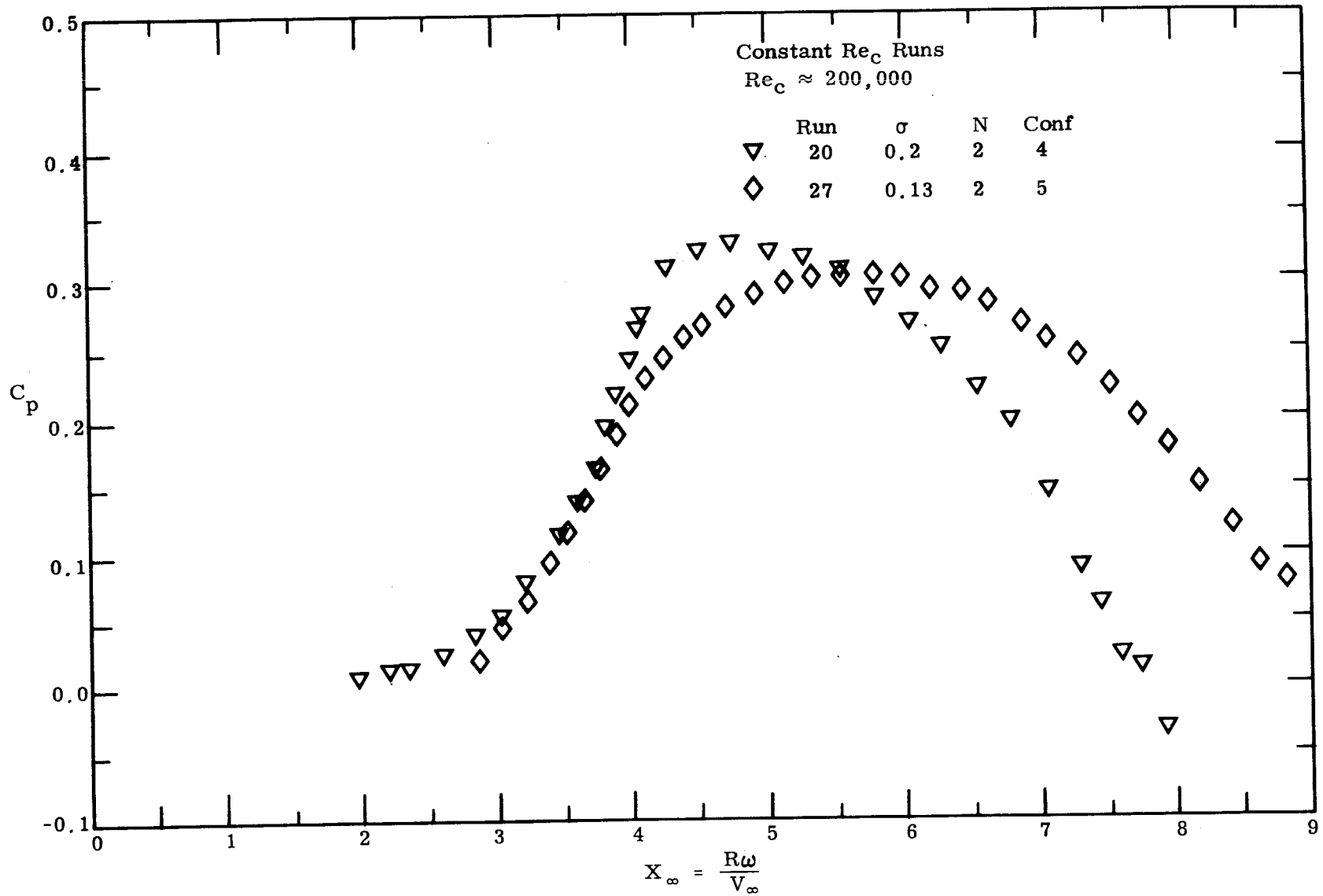

Figure 12. Effect of Solidity on Power Coefficient Data at Re$_c$ = 200,000

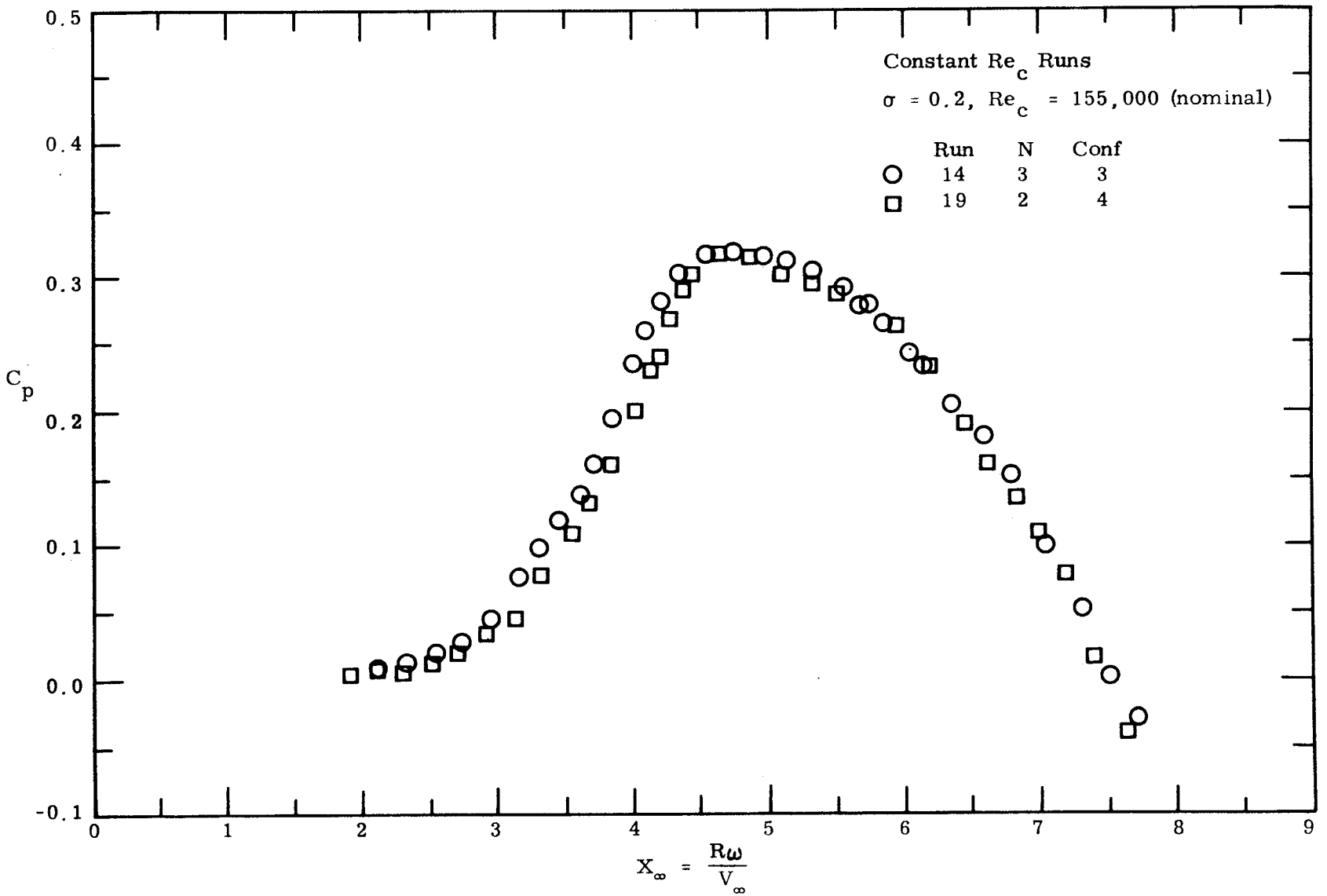

Figure 13. Effect of Number of Blades on Power Coefficient
Data at σ = 0.2 and Re$_c$ = 155,000

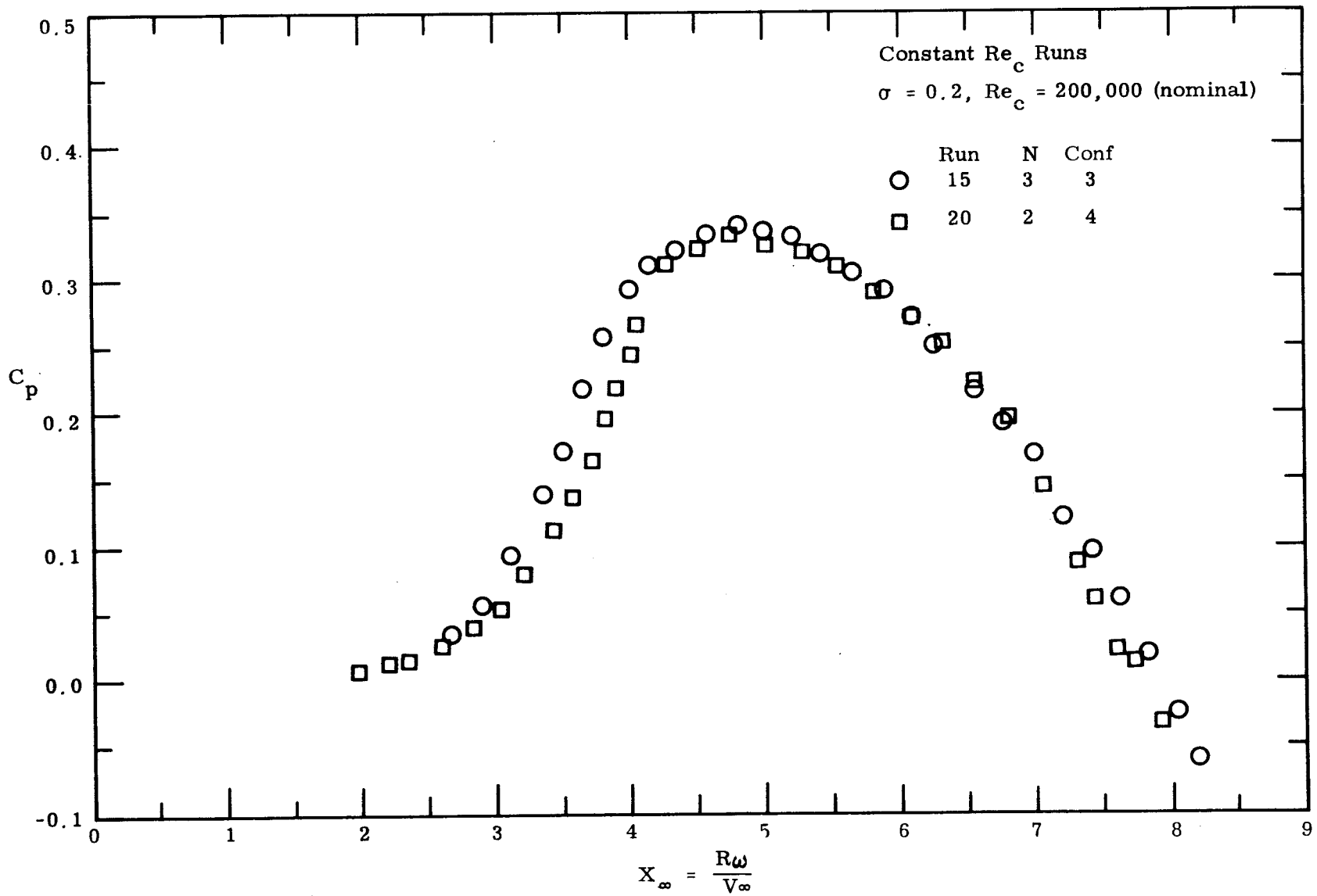

Figure 14. Effect of Number of Blades on Power Coefficient
Data at σ = 0.2 and Re$_c$ = 200,000

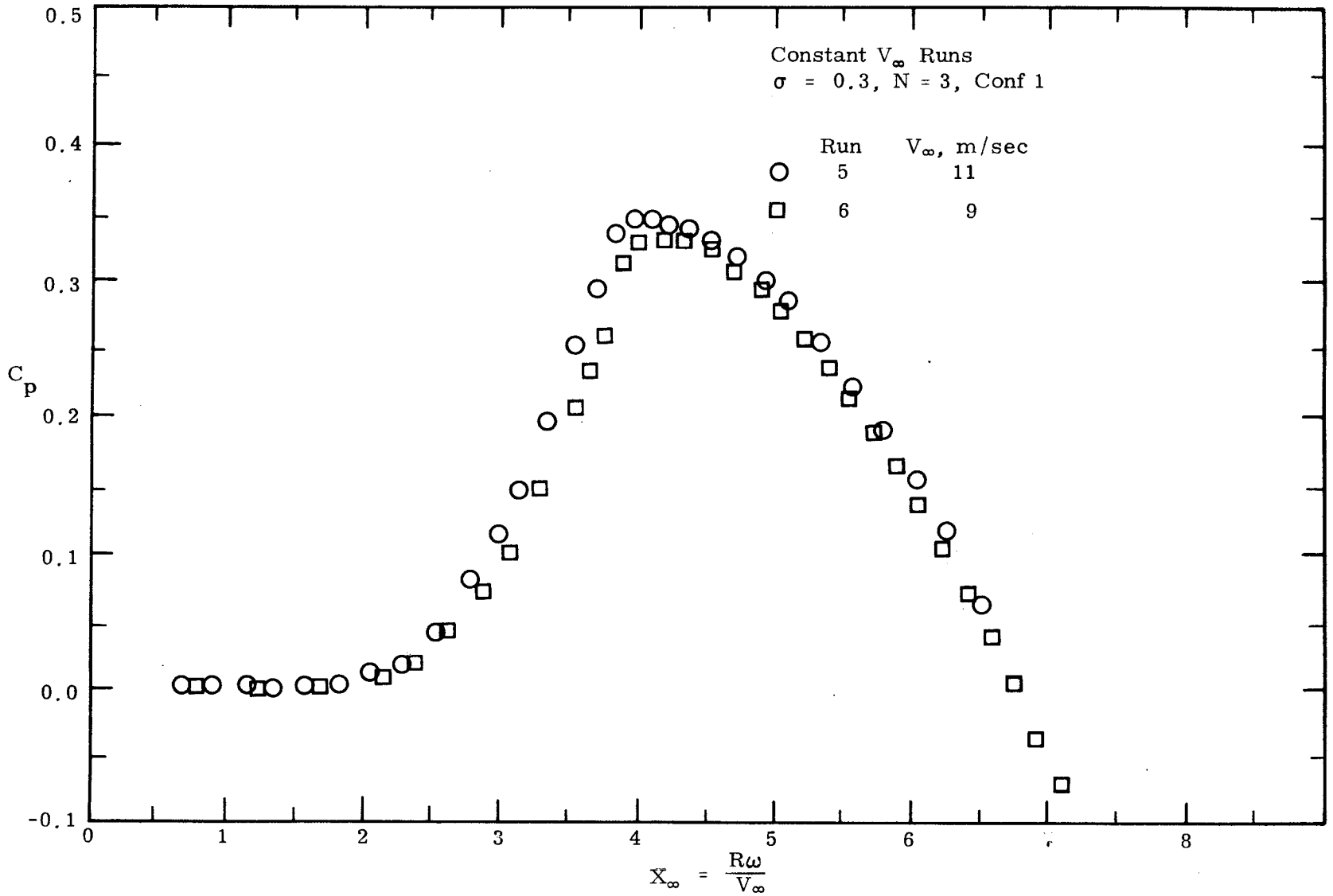

Figure 15. Power Coefficient Data for σ = 0.3, Constant Freestream Velocity

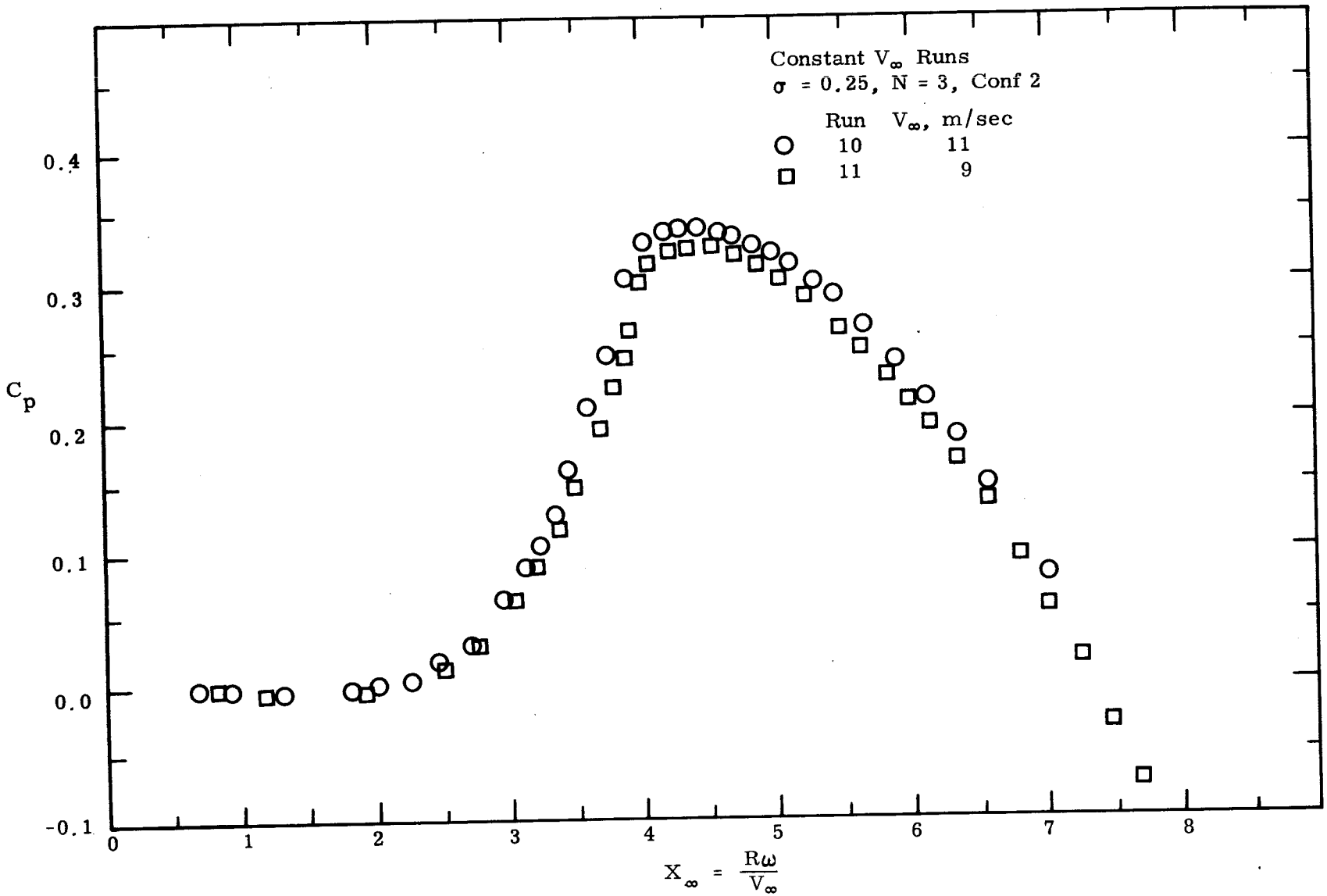

Figure 16. Power Coefficient Data for σ = 0.25, Constant Freestream Velocity

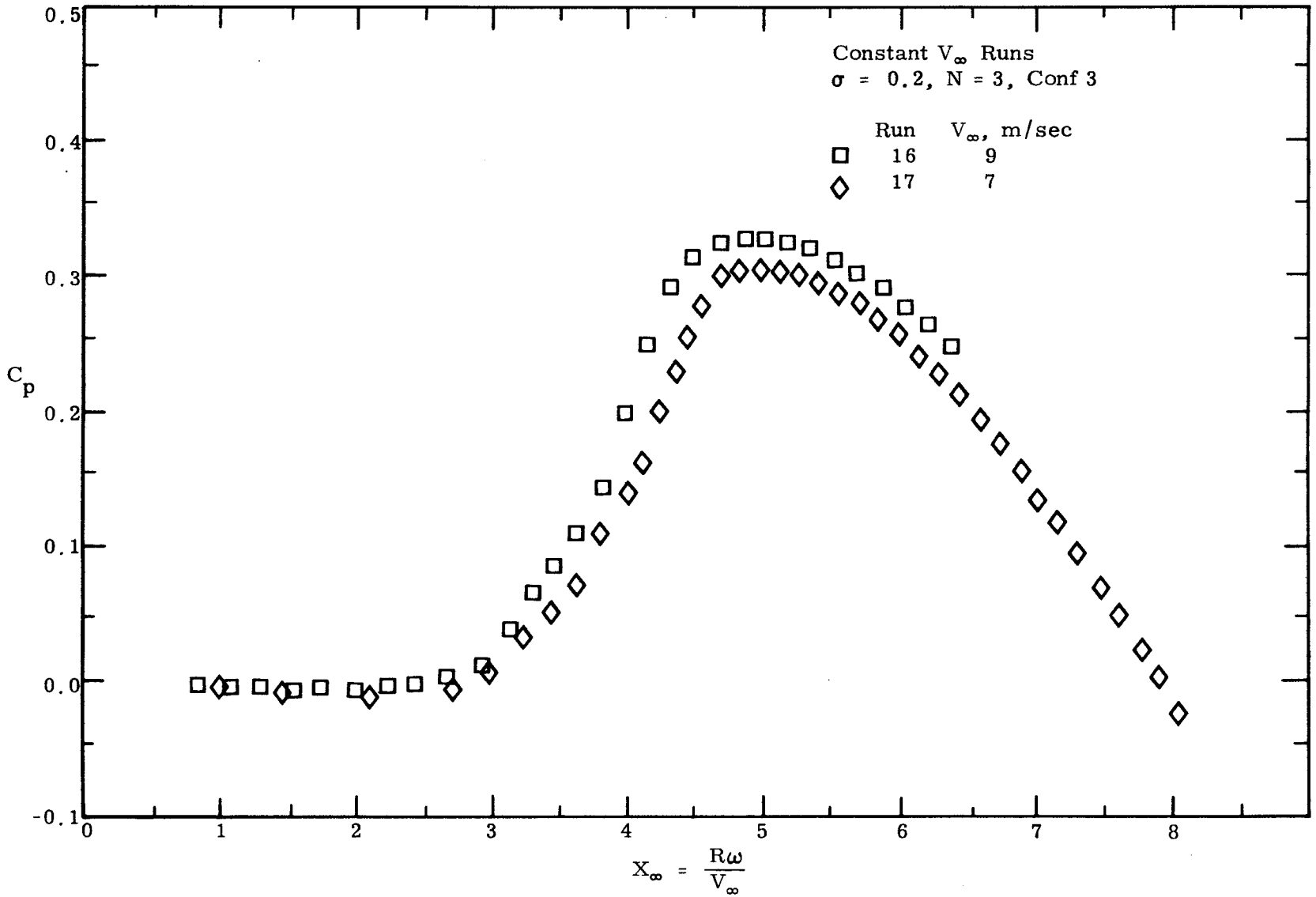

Figure 17. Power Coefficient Data for σ = 0.2, Constant Freestream Velocity (N = 3)

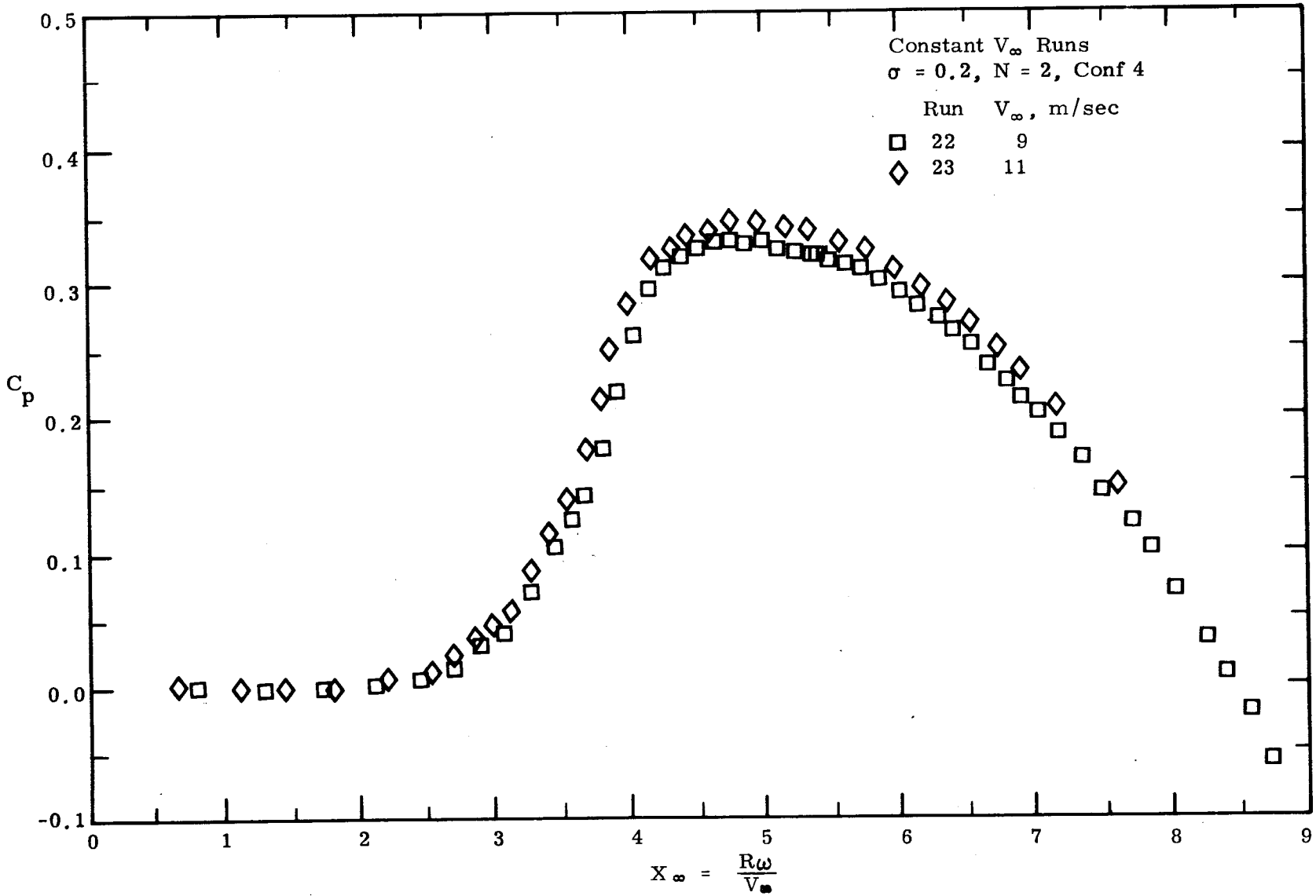

Figure 18. Power Coefficient Data for σ = 0.2, Constant Freestream Velocity (N = 2)

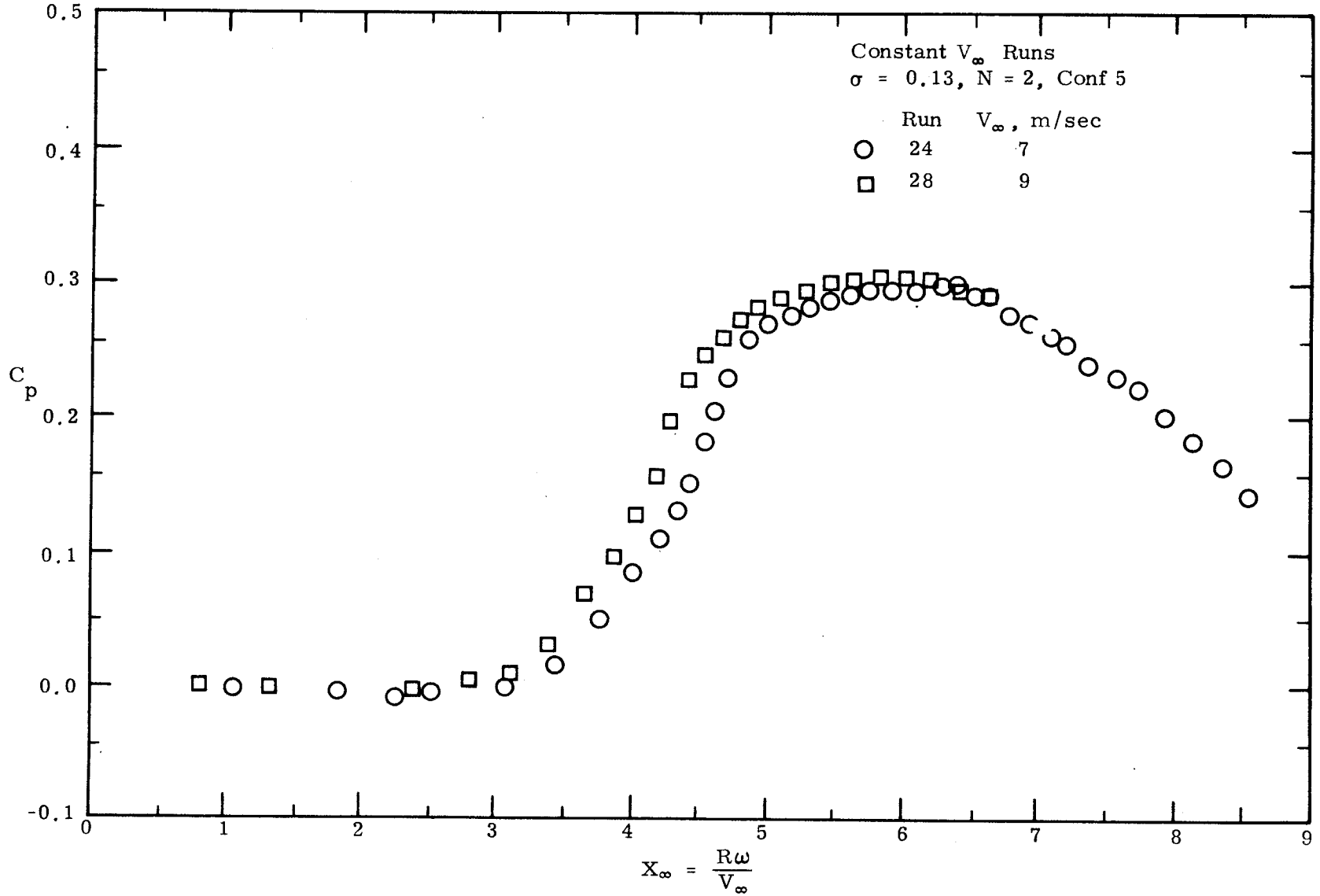

Figure 19. Power Coefficient Data for σ = 0.13, Constant Freestream Velocity

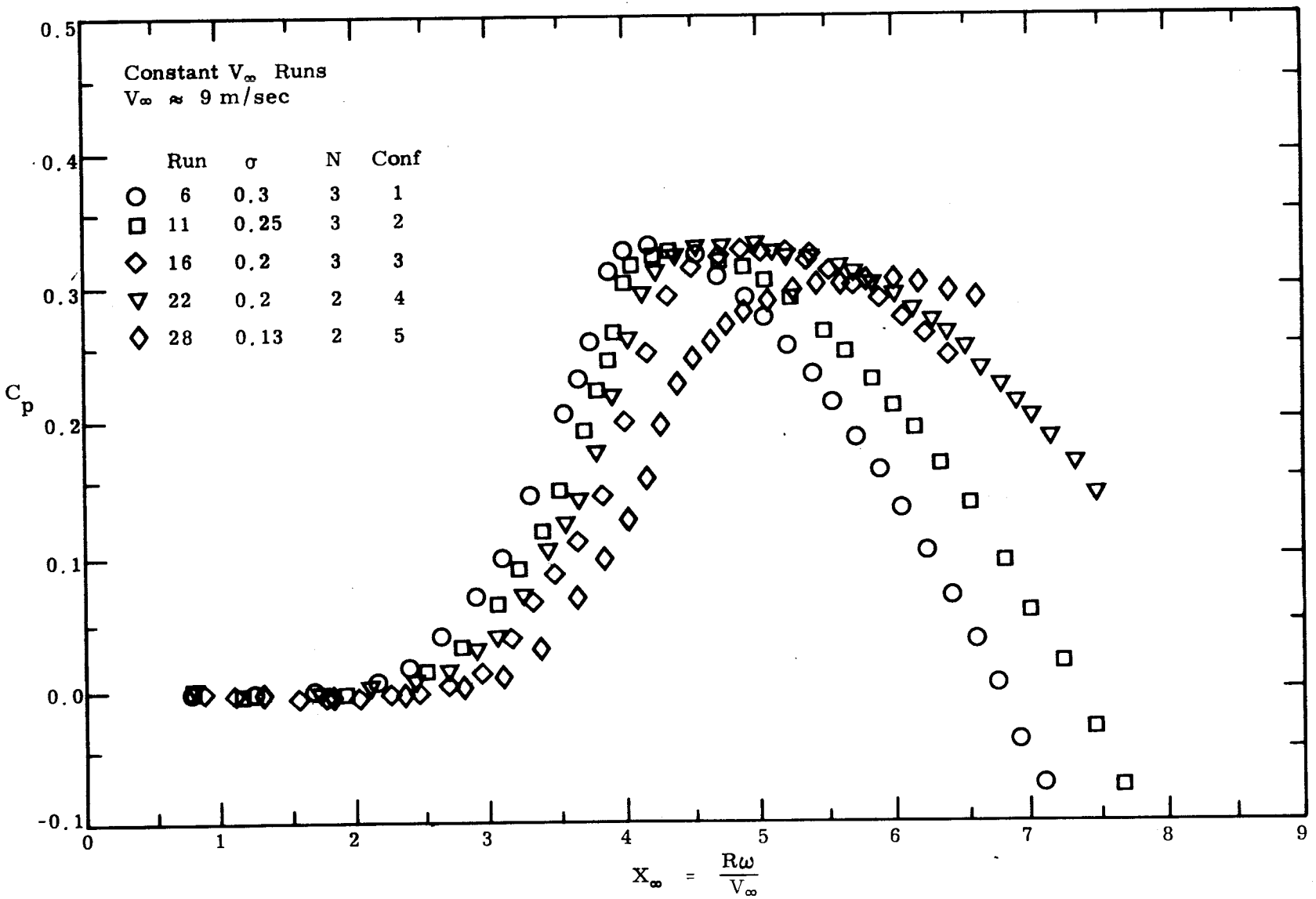

Figure 20. Effect of Solidity on Power Coefficient Data at V_∞ = 9 m/s

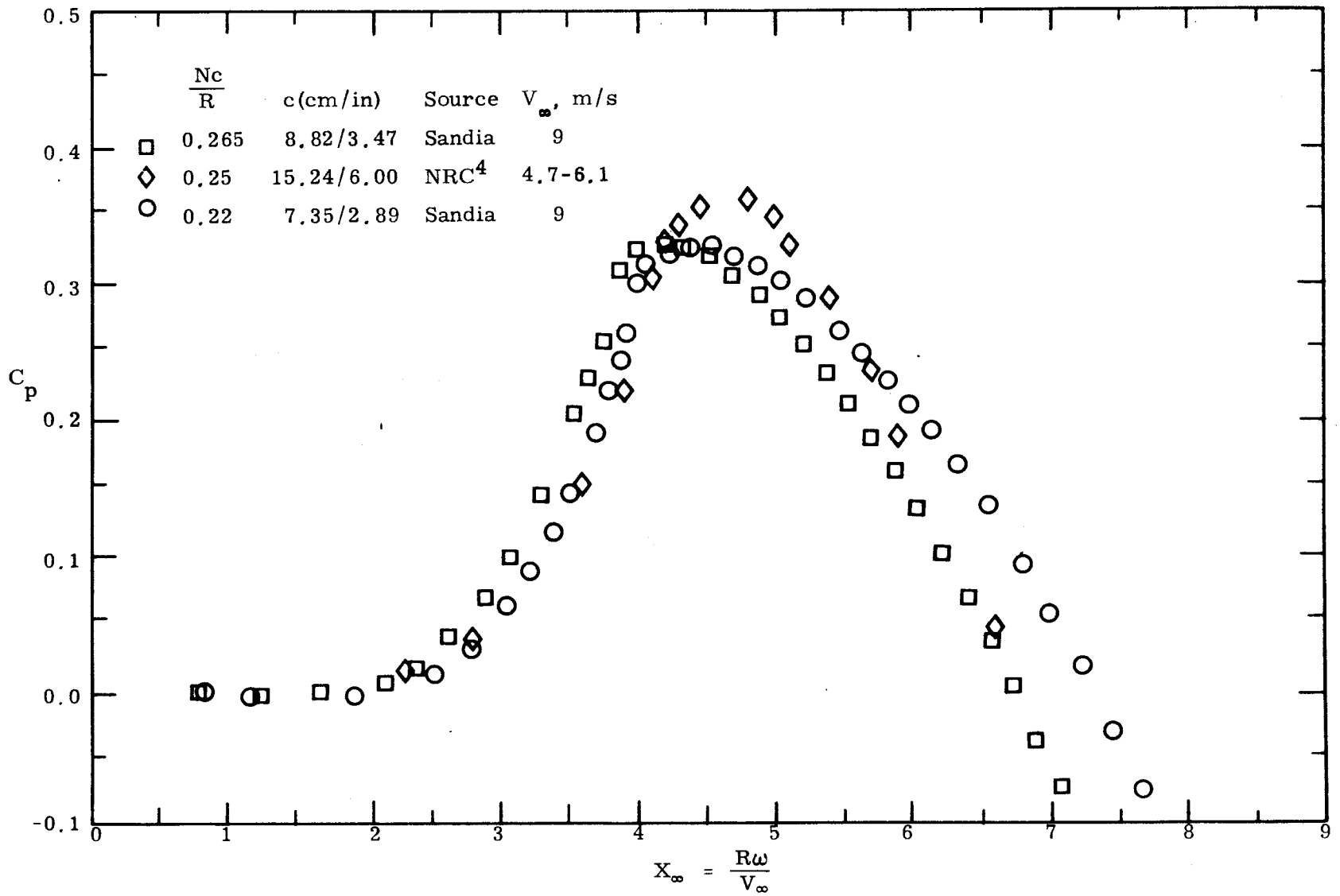

Figure 21. Comparison of Sandia and NRC Power Coefficient Data

APPENDIX

UNCERTAINTY ANALYSIS AND DATA REPEATABILITY

The method of Kline and McClintock[12] will be used to compute the experimental uncertainty associated with the power coefficient and tip-speed ratio calculations. The relationship that defines the power coefficient is

$$C_p \triangleq \frac{(Q + Q_f)\omega}{1/2\rho_\infty V_\infty^3 A_s} \quad . \tag{1}$$

The torque and rotational speed are both measured directly, whereas the freestream velocity is a function of the measured (and uncorrected) dynamic pressure and the tunnel blockage factor. These relationships are

$$V_\infty = V_{\infty_u}(1 + \epsilon_t) \tag{2}$$

and

$$V_{\infty_u} = \sqrt{\frac{2\, q_{\infty_u}}{\rho_\infty}} \quad . \tag{3}$$

The freestream density will be determined from the ideal gas law

$$\rho_\infty = \frac{P_\infty}{RT_\infty} \quad , \tag{4}$$

where the static pressure is computed from the sum of the barometric pressure and a gage pressure

$$P_\infty = P_{bar} + P_g \quad . \tag{5}$$

Substituting Eqs. (2)-(5) into Eq. (1), one obtains

$$C_p = \frac{\omega(Q + Q_f)}{2A_s q_{\infty_u}^{3/2}\left(1 + \epsilon_t\right)^3} \sqrt{\frac{P_{bar} + P_g}{RT_\infty}} \quad . \tag{6}$$

The power coefficient can be represented as a function of eight variables:

$$C_p = C_p(\omega,\ Q,\ Q_f,\ q_{\infty_u},\ \epsilon_t,\ P_{bar},\ P_g,\ T_\infty) \quad . \tag{7}$$

Following Kline and McClintock,[12] the uncertainty in the power coefficient (δC_p) can be written as:

$$\frac{\delta C_p}{C_p} = \left[\left(\frac{\delta\omega}{\omega}\right)^2 + \left(\frac{\delta Q}{Q + Q_f}\right) + \left(\frac{\delta Q_f}{Q + Q_f}\right)^2 + \left(\frac{3}{2}\,\frac{\delta q_{\infty_u}}{q_{\infty_u}}\right)^2 + \left(3\,\frac{\delta\epsilon_t}{1 + \epsilon_t}\right)^2 + \left(\frac{1}{2}\,\frac{\delta P_{bar}}{P_g + P_{bar}}\right) + \left(\frac{1}{2}\,\frac{\delta P_g}{P_g + P_{bar}}\right) + \left(\frac{1}{2}\,\frac{\delta T_\infty}{T_\infty}\right)^2\right]^{1/2} \quad . \tag{8}$$

It will be assumed that the uncertainty in swept area A_s is much smaller than that associated with the eight primary variables in Eq. (7).

Table A-1 tabulates the assumed uncertainties for this analysis. The majority of them are self-explanatory, but the torque and dynamic pressure require a few words of explanation. The calibration curve for the torque meter was linear to within 0.4 in-lbf; the indicator was accurate to within 0.3 in-lbf and can be read to within 0.1 in-lbf for a total of 0.8 in-lbf uncertainty. Reference 8 indicates that the tunnel dynamic pressure was uniform to within ±1.5 percent and that a prescribed value of the dynamic pressure can be set to within 0.017 psf.

TABLE A-I

Uncertainty in Primary Variables

Variable		Uncertainty
ω	rotation speed	$\delta\omega = 1$ rpm
Q	torque	$\delta Q = 0.8$ in-lbf
Q_f	friction torque	$\delta Q_f = 0.8$ in-lbf
q_{∞_u}	dynamic pressure	$\delta q_{\infty_u} = 0.015\, q_{\infty_u} + 0.017$ (psf)
ϵ_t	total blockage	$\delta_{\epsilon_t} = 0.5\, \epsilon_t = 0.013$, $\epsilon_t = 0.026$
P_{bar}	barometric pressure	$\delta P_{bar} = 0.02$ in-Hg $= 1.4$ psf
P_g	gage pressure	$\delta P_g = 1.5$ psf
T_∞	temperature	$\delta T_\infty = 1°F$

The assumed blockage uncertainty is constant for all runs, and the uncertainty associated with the freestream density is constant for all practical purposes. The above assumptions allow Eq. (8) to be written as

$$\frac{\delta C_p}{C_p} = \left[\left(\frac{\delta\omega}{\omega}\right)^2 + 2\left(\frac{\delta Q}{Q + Q_f}\right)^2 + \left(\frac{3}{2}\,\frac{\delta q_{\infty_u}}{q_{\infty_u}}\right)^2 + 0.00145\right]^{1/2} . \qquad (9)$$

The blockage uncertainty accounts for essentially all of the constant factor in Eq. (9); the sum of the squares of the density uncertainty terms is approximately 1.1×10^{-6}.

Several general conclusions can be drawn about the power coefficient uncertainty with the aid of Eq. (9) and Table A-I. The minimum achievable uncertainty is approximately 4.1 percent $\left(\sqrt{0.015^2 + 0.00145}\right)$, whereas the maximum percentage uncertainty can reach infinity at the point where $(Q + Q_f)$ is identically zero. For all cases, the uncertainty decreases with increasing rpm, torque, and dynamic

pressure. For the data of this report, the following approximate bounds can be established:

$$0.00167 < \frac{\delta\omega}{\omega} < 0.0167 \qquad 0.0000279 < \left(\frac{\delta}{\omega}\right)^2 < 0.000279$$

$$0.0025 < \frac{\delta q_{\infty_u}}{q_{\infty_u}} < 0.185 \qquad 0.0000141 < \left(\frac{3}{2}\frac{\delta q_{\infty_u}}{q_{\infty_u}}\right)^2 < 0.0770 \qquad (10)$$

$$-13.2 \le Q + Q_f \le 298.6 \text{ (in-lbf)} \quad .$$

From the above bounds, the uncertainty in rotational speed is not a major contributor to the uncertainty in power coefficient. For the constant rotational speed data, both low torque and low dynamic pressure occur simultaneously at the tip-speed ratios associated with runaway. Consequently, the uncertainty will be very high for the test condition of high tip-speed ratio and constant rotational speed.

One can perform a similar analysis for the uncertainty associated with the tip-speed ratio. From the definition of the tip-speed ratio, one can write

$$X_\infty = \frac{R\omega}{V_\infty}$$

$$= \frac{R\omega}{\sqrt{2}(1 + \epsilon_t)q_{\infty_u}^{1/2}} \left(\frac{P_g + P_{bar}}{RT_\infty}\right)^{1/2} \quad . \qquad (11)$$

The tip-speed-ratio relationship can be expressed functionally as follows:

$$X_\infty = X_\infty\left(\omega,\ q_{\infty_u},\ \epsilon_t,\ P_g,\ P_{bar},\ T_\infty\right) \quad . \qquad (12)$$

The fractional uncertainty can now be expressed as

$$\frac{\delta X_\infty}{X_\infty} = \left[\left(\frac{\delta\omega}{\omega}\right)^2 + \left(\frac{\delta q_{\infty_u}}{2q_{\infty_u}}\right)^2 + \left(\frac{\delta \epsilon_t}{1+\epsilon_t}\right)^2 + \left(\frac{1}{2}\,\frac{\delta P_g}{P_g + P_{bar}}\right)^2 + \left(\frac{1}{2}\,\frac{\delta P_{bar}}{P_g + P_{bar}}\right)^2 + \left(\frac{\delta T_\infty}{2T_\infty}\right)^2\right]^{1/2} . \tag{13}$$

Inserting the uncertainties that are approximately constant into Eq. (13), one obtains

$$\frac{\delta X_\infty}{X_\infty} = \left[\left(\frac{\delta\omega}{\omega}\right)^2 + \left(\frac{\delta q_{\infty_u}}{2q_{\infty_u}}\right)^2 + 0.000162\right]^{1/2} . \tag{14}$$

Utilizing Eqs. (9) and (13) in conjunction with the data in Table A-I, a complete uncertainty analysis was performed for some of the performance data for test configuration 1. The results of this analysis are shown in Figures A-1 and A-2 for the constant Reynolds number and constant freestream velocity test conditions, respectively. The bars around each data point represent the uncertainty bounds. For those data points that do not have the uncertainty bars, the uncertainty lies within the plotting symbol.

For the constant Reynolds number runs shown in Figure A-1, increasing the Reynolds number decreases the uncertainty for a given tip-speed ratio. The uncertainty in the low Reynolds number data (Run 1) is fairly large at the high tip-speed ratios. This is primarily due to the small dynamic pressure involved. Several data points in Figure A-1 were repeated, as indicated by the solid symbols. The degree of repeatability follows the trend of the uncertainty band quite well. The data scatter is very small for a given run; this indicates that the measurement errors are not of a random nature.

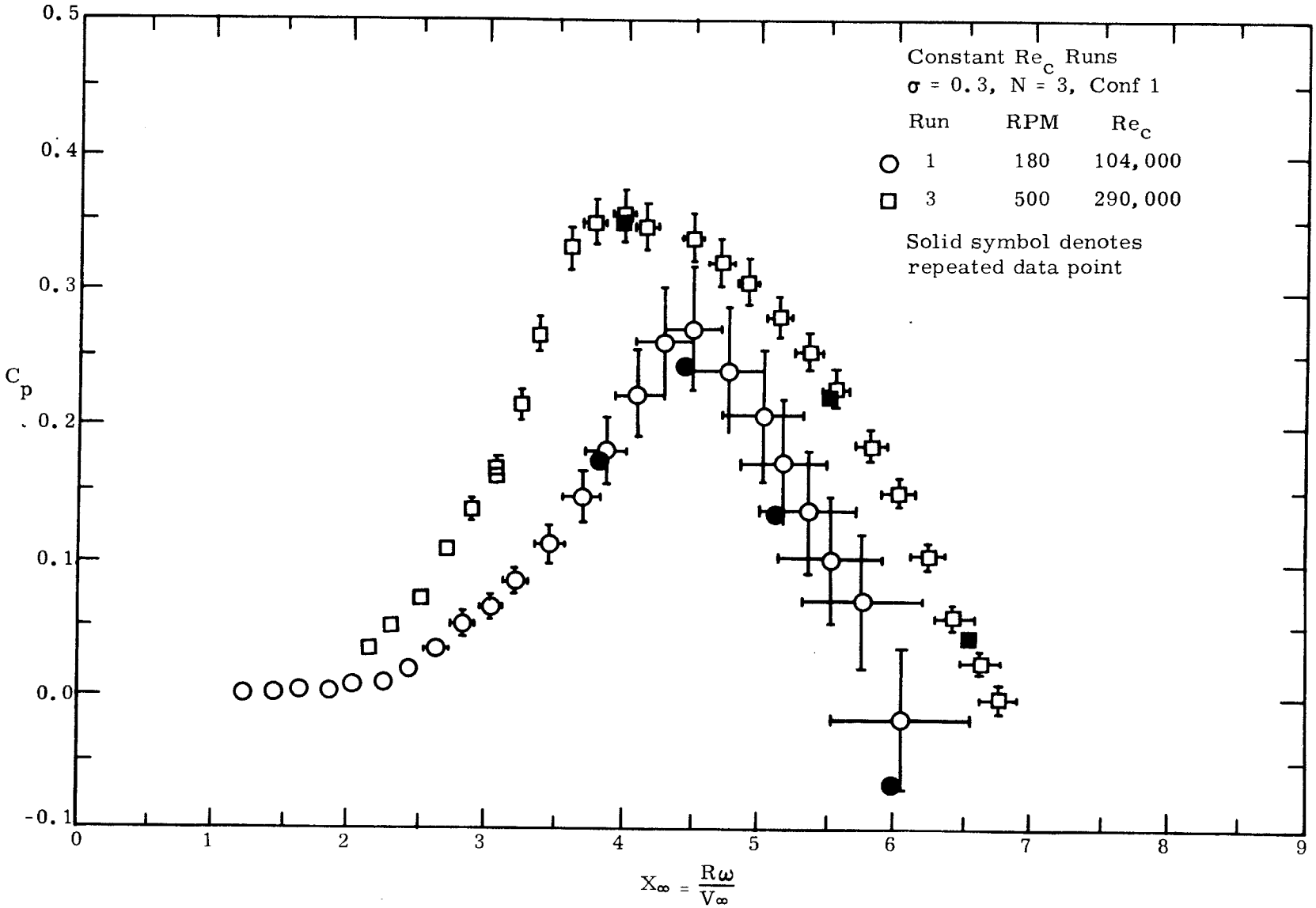

Figure A-1. Uncertainty Analysis for Representative Constant Reynolds Number Data

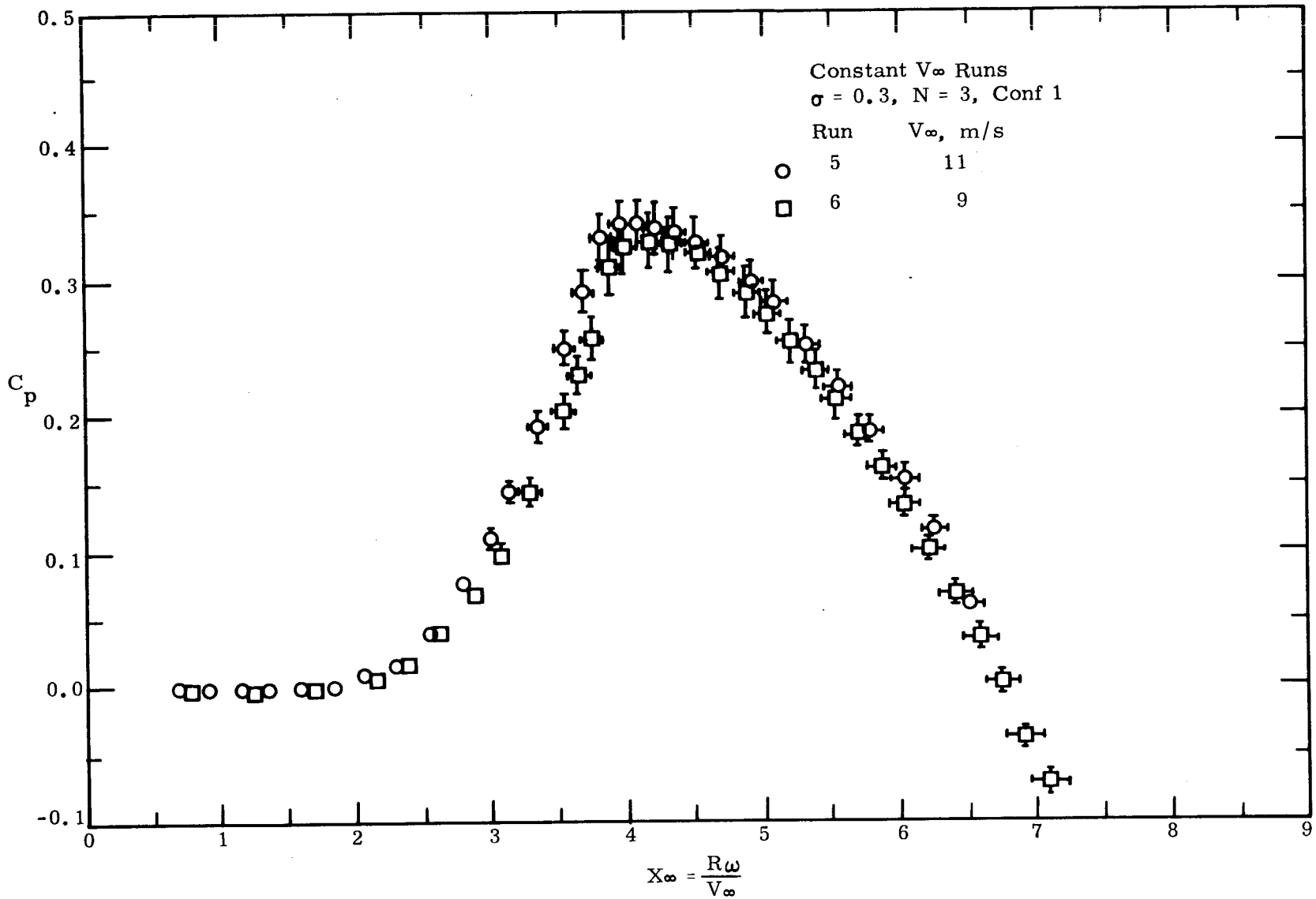

Figure A-2. Uncertainty Analysis for Representative Constant Freestream Velocity Data

For the constant freestream velocity runs shown in Figure A-2, increasing the freestream velocity decreases the uncertainty for a given tip-speed ratio. At low tip-speed ratios the absolute uncertainty in both C_p and X_∞ is small but the percentage uncertainty is relatively large.

The uncertainty trends presented for test configuration 1 should be taken as being representative of the other configurations tested.

REFERENCES

1. P. South and R. S. Rangi, Preliminary Tests of a High Speed - Vertical Axis Windmill Model, National Research Council of Canada, LTR-LA-74, March 1971.
2. P. South and R. S. Rangi, A Wind Tunnel Investigation of a 14-ft Diameter Vertical-Axis Windmill, National Research Council of Canada, LTR-LA-105, September 1972.
3. P. South and R. S. Rangi, "The Performance and Economics of the Vertical-Axis Wind Turbine Developed at the National Research Council, Ottawa, Canada," Agricultural Engineer, February 1974, pp. 14-16. (See also American Society of Agricultural Engineers, Paper No. PNW 73-303).
4. R. J. Templin, Aerodynamic Performance Theory for the NRC Vertical-Axis Wind Turbine, National Research Council of Canada, LTR-LA-160, June 1974.
5. G. E. Reis and B. F. Blackwell, Practical Approximations to a Troposkien by Straight-Line and Circular-Arc Segments, Sandia Laboratories, SAND74-0100, March 1975.
6. B. F. Blackwell and G. E. Reis, Blade Shape for a Troposkien Type of Vertical-Axis Wind Turbine, Sandia Laboratories, SLA-74-0154, April 1974.
7. B. F. Blackwell and G. E. Reis, Some Geometrical Aspects of Troposkiens as Applied to Vertical-Axis Wind Turbines, Sandia Laboratories, SAND74-0177, May 1975.
8. J. W. Holbrook, Low Speed Wind Tunnel Handbook, LTV Aerospace, AER-EOR-12995-B, February 1974.
9. J. F. Banas, E. G. Kadlec, and W. N. Sullivan, Methods for Performance Evaluation of Synchronous Power Systems Utilizing the Darrieus Vertical-Axis Wind Turbine, Sandia Laboratories, SAND75-0204, April 1975.
10. Alan Pope and John J. Harper, Low Speed Wind Tunnel Testing, New York: John Wiley & Sons, Inc., 1966.
11. J. H. Strickland, The Darrieus Turbine: A Performance Prediction Model Using Multiple Streamtubes, Sandia Laboratories, SAND75-0431, October 1975.
12. S. J. Kline and F. A. McClintock, "Describing Uncertainties in Single-Sample Experiments," Mech. Eng., January 1953, p. 3.

DISTRIBUTION:

TID-4500-R64, UC-60 (249)

R. J. Templin
Low Speed Aerodynamics Section
NRC-National Aeronautical Establishment
Ottawa 7, Ontario, Canada K1AOR6

A. Robb
Memorial Univ. of Newfoundland
Faculty of Eng. & Applied Sciences
St. John's Newfoundland
Canada A1C 5S7

H. Sevier
Rocket and Space Division
Bristol Aerospace Ltd.
P. O. Box 874
Winnipeg, Manitoba
R3C 2S4 Canada

V. A. L. Chasteau
Department of Mech. Engineering
The University of Auckland
Private Bag
Auckland, New Zealand

G. Herrera
Jet Propulsion Lab
4800 Oak Grove Drive
Pasadena, CA 91103

NASA Langley Research Center
Hampton, VA 23365
Attn: R. Muraca, MS 317

NASA Lewis Research Center (2)
2100 Brookpark Road
Cleveland, OH 44135
Attn: J. Savino, MS 500-201
R. L. Thomas

ERDA Headquarters (20)
Washington, DC 20545
Attn: L. Divone

University of New Mexico (2)
Albuquerque, NM 87131
Attn: K. T. Feldman
Energy Research Center
V. Sloglund
ME Department

A. V. da Rosa
Stanford Electronic Laboratories
Radio Science Laboratory
Stanford, CA 94305

A. N. L. Chiu
Wind Engineering Research Digest
Spalding Hall 357
University of Hawaii
Honolulu, HI 96822

R. N. Meroney
Colorado State University
Dept. of Civil Engineering
Fort Collins, CO 80521

A. G. Vacroux
Illinois Institute of Technology
Dept. of Electrical Engineering
Chicago, IL 60616

Oklahoma State University (2)
Stillwater, OK 74074
Attn: W. L. Hughes
EE Department
D. K. McLaughlin
ME Department

Oregon State University (2)
Corvallis, OR 97330
Attn: R. Wilson
ME Department
R. W. Thresher
ME Department

Texas Tech University (3)
Lubbock, TX 79409
Attn: K. C. Mehta, CE Dept.
J. Strickland, ME Dept.
J. Lawrence, ME Dept.

R. G. Watts
Tulane University
Dept. of Mechanical Engineering
New Orleans, LA 70018

Aero Engineering Department (2)
Wichita State University
Whichita, KS 67208
Attn: M. Snyder
Bill Wentz

DISTRIBUTION (cont):

Nevada Operations Office, ERDA (2)
P. O. Box 14100
Las Vegas, NV 89114
Attn: R. Ray, Operations
H. Mueller, ARL

Los Alamos Scientific Lab (7)
P. O. Box 1663
Los Alamos, NM 87544
Attn: R. R. Brownlee, J-9
J. R. Bartlit, Qu-26
J. D. Balcomb, Q-DO-T
R. G. Wagner, P-5
J. Nachamkin, T-DO-TEC
S. W. Depp. E-DO
H. Deinken, ADWP-1

ERDA/ALO (3)
Kirtland AFB East
Albuquerque, NM 87115
Attn: D. K. Knowlin
D. C. Graves
D. W. King

R. Camerero
Faculty of Applied Science
University of Sherbrooke
Sherbrooke, Quebec
Aanada J1K 2R1

American Wind Energy Association
21243 Grand River
Detroit, MI 48219

E. E. Anderson
Dept. of Mechanical Engineering
South Dakota Sch. of Mines & Tech.
Rapid City, SD 57701

E. S. Takle
Climatology and Meteorology
312 Curtiss Hall
Iowa State University
Ames, IA 50011

P. B. S. Lissaman
Aeroenvironment, Inc.
660 South Arroya Parkway
Pasadena, CA 991105

R. A. Parmelee
Department of Civil Engineering
Northwestern University
Evanston, IL 60201

J. Park
Helion
P. O. Box 4301
Sylmar, CA 91342

W. F. Foshag
Aerophysics Company
3500 Connecticut Avenue NW
Washington, DC 20008

W. L. Harris
Aero/Astro Department
MIT
Cambridge, MA 02139

K. Bergey
Aero Engineering Department
University of Oklahoma
Norman, OK 73069

J. Fischer
F. L. Smidth & Company A/S
Vigerslevalle 77
2500 Valby, Denmark

H. M. Busey
DMA, Safety and Facilities A-364
ERDA Headquarters
Washington, DC 20545

P. Bailey
P. O. Box 3
Kodiak, AK 99615

M. E. Beecher
Solar Energy Collection
Arizona State University
University Library
Tempe, AZ 85281

U. A. Coty
Lockheed - California Co.
Box 551-63A1
Burbank, CA 91520

DISTRIBUTION (cont):

Lawrence Livermore Laboratory (2)
P. O. Box 808 L-340
Livermore, CA 94550
Attn: D. W. Dorn
D. Hardy

J. A. Garate
General Electric
Valley Forge Space Center
King of Prussia, PA 19406

O. Krauss
Division of Engineering Research
Michigan State University
East Lansing, MI 48823

P. Calnan
Electrical Research Associates
Cleeve Road
Leatherhead,
Surrey, England

V. Nelson
Department of Physics
West Texas State University
P. O. Box 248
Canyon, TX 79016

E. Gilmore
Amarillo College
Amarillo, TX 79100

R. K. Swanson
Southwest Research Institute
San Antonio, TX 78284

L. Lliljdahl
Building 303
Agriculture Research Center
USDA
Beltsville, MD 20705

T. Wentink, Jr.
Geophysical Institute
University of Alaska
Fairbanks, AK 99701

E. J. Warchol
Bonneville Power Administration
P. O. Box 3621
Portland, OR 97225

W. Batesole
Kaman Aerospace Corporation
Bloomfield, CT 06002

D. Lindley
Mechanical Engineering
University of Canterbury
Christchurch, New Zealand

Olle Ljungstrom
Swedish Board for Tech. Development
FACK
S-100 72 Stockholm 43, Sweden

Robert Brulle
McDonnell-Douglas
P. O. Box 516
Dept. 241, Bldg. 32
St. Louis, MO 63166

Richard Walters
W. Va. University
1062 Kountz Ave
Morgantown, WV 26505

Albert Fritzsche
Dornier System GmbH
Postfach 1360
7990 Friedrichshafen
West Germany

P. N. Shankar
Aerodynamics Division
National Aeronautical Laboratory
Bangalore 560017
India

Peter Andersen
Karstykket 42
Vvelse 3550
Slangerup, Denmark

Otto de Vries
National Aerospace Laboratory
Anthony Fokkerweg 2
Amsterdam 1017
The Netherlands

J. P. Johnston
Mechanical Engineering
Stanford University
Stanford, CA 94305

DISTRIBUTION:

Lt T. Colburn
USCG R&D Center
Avory Point
Groton, CT 06340

James Meiggs
Kaman Sciences Corp.
P.O. Box 7463
Colorado Springs, CO 80933

G. P. Hawkins
Irwin Industries
6045 West 55th Place
Arvada, CO 80002

Don Greider
Solar Central
7213 Ridge Rd.
Mechanicsburg, OH 43044

D. G. Shepherd
Sibley School of Mechanical
and Aerospace Engineering
Cornell University
Ithaca, NY 14853

1000 G. A. Fowler
1200 W. A. Gardner
1284 W. N. Sullivan
1284 L. I. Weingarten
1300 D. B. Shuster
1320 M. L. Kramm
1324 E. C. Rightley
Attn. D. F. McNeill
1324 L. V. Feltz
1330 R. C. Maydew
1333 S. McAlees, Jr.
1333 B. F. Blackwell (100)
1333 R. E. Sheldahl
1400 A. Y. Pope
5000 A. Narath
5431 D. W. Lobitz
5443 J. W. Reed
5700 J. H. Scott
5710 G. E. Brandvold
5715 R. H. Braasch
5715 E. G. Kadlec (100)
5715 R. C. Reuter
5715 A. F. Veneruso
5742 J. F. Banas
8000 T. B. Cook, Jr.
8100 L. Gutierrez
8110 A. N. Blackwell
8300 B. F. Murphey
8320 T. S. Gold
8266 E. A. Aas (2)
3141 C. A. Pepmueller (Actg) (5)
3151 W. L. Garner (3)
For ERDA/TIC (Unlimited Release)

DISTRIBUTION:
(Second Printing March 1977)

1333 B. F. Blackwell (100)